Chem Soc Rev

REVIEW ARTICLE

View Article Online
View Journal | View Issue

Cite this: *Chem. Soc. Rev.*, 2017, **46**, 3770

Photoprotection: extending lessons learned from studying natural sunscreens to the design of artificial sunscreen constituents

Lewis A. Baker,[a] Barbara Marchetti,[b] Tolga N. V. Karsili,*[c] Vasilios G. Stavros*[a] and Michael N. R. Ashfold *[d]

Evolution has ensured that plants and animals have developed effective protection mechanisms against the potentially harmful effects of incident ultraviolet radiation (UVR). Tanning is one such mechanism in humans, but tanning only occurs post-exposure to UVR. Hence, there is ever growing use of commercial sunscreens to pre-empt overexposure to UVR. Key requirements for any chemical filter molecule used in such a photoprotective capacity include a large absorption cross-section in the UV-A and UV-B spectral regions and the availability of one or more mechanisms whereby the absorbed photon energy can be dissipated without loss of the molecular integrity of the chemical filter. Here we summarise recent experimental (mostly ultrafast pump–probe spectroscopy studies) and computational progress towards unravelling various excited state decay mechanisms that afford the necessary photostability in chemical filters found in nature and those used in commercial sunscreens. We also outline ways in which a better understanding of the photophysics and photochemistry of sunscreen molecules selected by nature could aid the design of new and improved commercial sunscreen formulations.

Received 11th February 2017

DOI: 10.1039/c7cs00102a

rsc.li/chem-soc-rev

[a] *Department of Chemistry, University of Warwick, Gibbet Hill Road, Coventry, CV4 7AL, UK. E-mail: v.stavros@warwick.ac.uk*
[b] *Department of Chemistry, University of Pennsylvania, Philadelphia, USA*
[c] *Department of Chemistry, Temple University, Philadelphia, USA. E-mail: tug96217@temple.edu*
[d] *School of Chemistry, University of Bristol, Cantock's Close, Bristol, BS8 1TS, UK. E-mail: mike.ashfold@bristol.ac.uk*

1. Introduction

The causal link between excessive sun exposure and the development of skin erythema and tanning has been known for millennia, even if the reason for this link has only begun to be understood much more recently. Ancient civilisations, such as the Egyptians and the Greeks, took steps to protect themselves with varying

Lewis A. Baker

Lewis Baker studied Physics at the University of Warwick, obtaining an MPhys in 2013. He went on to study Mathematical Biology and Biophysical Chemistry at the University of Warwick Molecular Organisation and Assembly in Cells Doctoral Training Centre, obtaining an MSc in 2014 and proceeding to a PhD with Drs Vasilios Stavros and Scott Habershon. His thesis focusses on understanding biological photoprotection through transient absorption spectroscopy and quantum dynamic simulations.

Barbara Marchetti

Barbara Marchetti obtained her undergraduate Bachelor and Masters degrees at the Università degli Studi di Perugia, Italy in 2010 and 2012, respectively. She completed her PhD degree at the University of Bristol in 2016 under the supervision of Prof. Michael Ashfold and will commence a Marie Skłodowska Curie international Post-Doctoral Research Fellowship in the group of Prof. Marsha Lester at the University of Pennsylvania, USA in the spring of 2017. Her research interests comprise the photochemistry and photophysics of biologically, catalytically and environmentally relevant chromophores.

success; rice bran, jasmine and olive oil were applied to the skin, often for cosmetic reasons, but these formulations also provided some photoprotection and are thus amongst the earliest recorded sunscreens.[1–3] Other landmark discoveries in this field include the identification of ultraviolet (UV) radiation (UVR) by Ritter (in 1801) and the experiments of Widmark in 1889 proving that UVR caused erythema solare (sunburn); suggestions to use chemical sunscreens in order to protect the skin were already gaining traction by the end of the 19th century.[4–6]

One of the first successful commercial sunscreen products was developed by Schueller (in 1935), who went on to found the company now known as L'Oreal. The sunscreen was called 'Ambre Solaire', an oily substance containing the UV absorber benzylsalicylate. In subsequent years many other potential compounds were investigated spectroscopically, leading to the widespread adoption of *para*-aminobenzoic acid[4,6–10] and, later, benzophenones.[11] By now, many dozens of UV absorbing molecules find regular use in commercial products,[12–14] which fuel a global industry, and international regulations control both the identities and the concentrations of specific UV absorbing molecules approved for use in such products. These regulations have developed, in part, as a result of concerns that some of the sunscreen components might have an adverse effect on the human skin or physiology. These concerns, often referred to as the 'sunscreen controversy',[12,15] have caused a surge of research focussed on gaining a deeper understanding of how sunscreen constituents operate and provide photoprotection. Through understanding such photoprotective mechanisms, we might hope to learn lessons about the properties of what constitutes a good sunscreen molecule and, ultimately, apply this knowledge to the design of new or improved compounds.

The remainder of this Introduction overviews some of the ways photoprotection is achieved in nature and then outlines ways in which we can alleviate the deleterious effects of UVR. This is followed by a further four sections. The first is a short photochemistry primer, wherein we introduce photoexcited states and some of the many possible decay mechanisms for excited state molecules, then focus on mechanisms that enable (ultrafast) population transfer back to the starting ground state configuration – a key requirement for a chemical filter suitable for use in a commercial sunscreen. We then survey some of the contemporary experimental and theoretical methods by which the early time dynamics of photoexcited molecules can be probed and understood. This is followed by a description of several recent case studies of the ultrafast decay of natural and commercial molecular sunscreen components. Finally, we outline various experimental and theoretical prospects that can be expected to enhance this currently rather small but fast growing field of study.

Tolga N. V. Karsili

Tolga Karsili obtained his MSci degree from the University of Birmingham in 2010 and his PhD in 2014 from the University of Bristol, where he worked in the group of Prof. Michael Ashfold. He then undertook post-doctoral research in the Computational and Theoretical Chemistry group at the Technical University of Munich, Germany (supported in part by the award of a T. U. Munich Fellowship), and is now a research fellow at Temple University, USA. His research interests involve the photodynamics of organic and biological chromophores, supramolecular photochemistry and electron-induced reactions – in both the gas phase and in bulk solution.

Natural photoprotection

The UV wavelengths are the most energetic part of the solar spectrum reaching the surface of the Earth. These are usually

Vasilios G. Stavros

Vasilios Stavros is a Reader at the University of Warwick. He completed his PhD in 1999 at King's College London, working in the group of Prof. Helen Fielding and remained at King's for a further three years as an EPSRC postdoctoral research fellow. In 2002, he undertook a postdoctoral position at the University of California Berkeley, working for Prof. Stephen Leone. He returned to the UK in 2005 as a Royal Society University Research Fellow. His research is centred on understanding photoprotection and photoactivation mechanisms in biologically related molecules using both gas- and solution-phase pump–probe spectroscopies.

Michael N. R. Ashfold

Mike Ashfold obtained his PhD degree in 1978 at the University of Birmingham in the group of Prof. John Simons. After postdoctoral research at the University of Oxford, he was appointed as a Lecturer at the University of Bristol, where he was promoted to a Chair in Physical Chemistry in 1992. He was elected to the Fellowship of the Royal Society in 2009. His research interests include molecular photophysics, spectroscopy, and plasma diagnosis (particularly in the context of diamond chemical vapour deposition).

sub-divided into three regions: UV-A (spanning the wavelength range 400–315 nm), UV-B (315–280 nm) and UV-C (280–100 nm). UV-C radiation is now almost completely absorbed and scattered by our ozone-rich atmosphere, but it has not always been so. In the early Archean period of the Earth's history (some 4 billion years ago), the atmosphere was dominated by carbon dioxide and nitrogen. The concentration of oxygen was very low.[18] Thus there was nothing to attenuate the higher energy (UV-C) components within the solar spectrum prior to their reaching the Earth's surface. Early organisms (*e.g.* phototrophs) developing in these harsh conditions thus had two choices. One was to migrate away from the surface. The other was to develop protection mechanisms whereby damage from the short wavelength components within the incident solar radiation was minimised, whilst the longer wavelength components required for photosynthesis could still be harnessed. Similar selective pressures may well have led to many of the DNA-repair mechanisms observed in present-day organisms.[19,20] This is a classic example of the so-called burden of disease,[21] where solar radiation is required for photosynthesis, but can also lead to damage. Thus some equilibrium needs to be struck.

A similar balance with regard to UVR exposure continues to exist across the Earth's biosphere – as illustrated by the burden of disease curve (for humans and plants) shown in Fig. 1. We start by considering the effects of UVR exposure and physiological responses in humans. More than 90% of the body's vitamin D requirements are satisfied by the UV-B mediated conversion of 7-dehydrocholesterol to previtamin D_3, a precursor of vitamin D.[22] Underexposure to UV-B can thus lead to a deficiency in vitamin D, which can lead to the development of skeletal disease and osteoporosis.[22,23] Conversely, overexposure to UVR is the primary cause of skin cancers, *e.g.* basal and squamous cell carcinomas, and malignant melanomas. The latter are estimated to be responsible for some 55 000 fatalities world-wide, annually.[21] Overexposure to UVR is also deemed responsible for some 3 million cases of cataracts per year, globally, and has even been linked to some mental illnesses.[21]

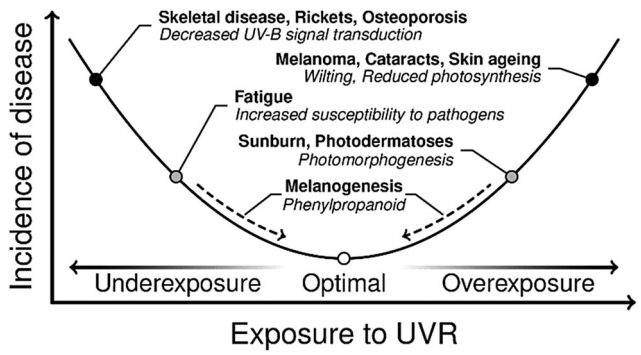

Fig. 1 A burden of disease curve exhibited by humans and plants in response to exposure to UVR. There are a number of ailments due to acute and chronic under or overexposure to UVR. Gene-regulated pathways (dashed arrows) exist to respond to changing UVR exposure in order to perturb the incidence of disease to a minimum. This figure is adapted from ref. 24.

The body has many mechanisms in place to reduce the effects of UVR exposure. For example, DNA checkpointing and repair processes can identify and rectify much of the damage caused by UVR.[20,25] But these are post-UVR damage processes. The primary photoprotective mechanism is skin pigmentation which, among its many physiological roles,[26,27] reduces UVR damage occurring in the first place. Human skin pigmentation consists of a class of UV absorbing molecules termed melanins. These sub-divide into eumelanin, a black-brown pigment, pheomelanin, a reddish-yellow pigment, and neuromelanin, a dark brown pigment found only in the brain.[26,27] Eumelanin and pheomelanin (particularly the former) are mainly responsible for photoprotection against UVR, and we henceforth focus on these pigments.

Eumelanin and pheomelanin, the structures of which are shown in Fig. 2, are synthesised through a tyrosine-driven biochemical pathway. Tyrosine is first converted to dopaquinone enzymatically. If no cysteine is present, dopaquinone can be converted to dihydroxyindole or dihydroxyindole carboxylic acid. These polymerise to form eumelanin. In the presence of cysteine, however, dopaquinone is converted to isomers of cysteinyldopa before forming benzothiazine intermediates, which polymerise to form pheomelanin.[28,29]

As Fig. 3 shows, specialised cells termed melanocytes are distributed throughout the stratum basale layer.[30] These synthesise vesicles termed melanosomes which, in turn, synthesise melanin.[30,31] Melanocytes form long projections (dendrites) out to surrounding skin keratinocytes (the dominant cell type in the epidermis) in the stratum basale and stratum spinosum layers; typically, one melanocyte reaches upwards of 40 keratinocytes.[32] Melanin-containing melanosomes are transferred to the ends of the dendrites through cytoskeletal assisted processes, and

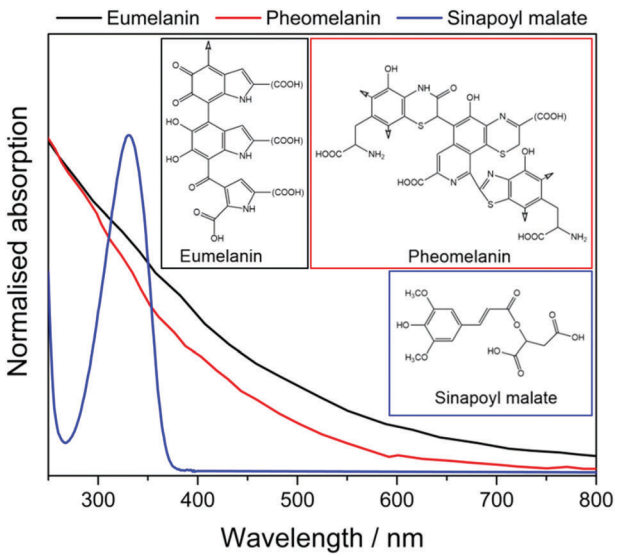

Fig. 2 The UV-visible absorption spectra of eumelanin (black) and pheomelanin (red) in water.[16] The high degrees of polymerisation of the chromophores give both pigments a broad absorption profile. Sinapoyl malate (blue) in dioxane,[17] on the other hand exhibits a relatively narrow absorption band, mostly in the UV-B region.

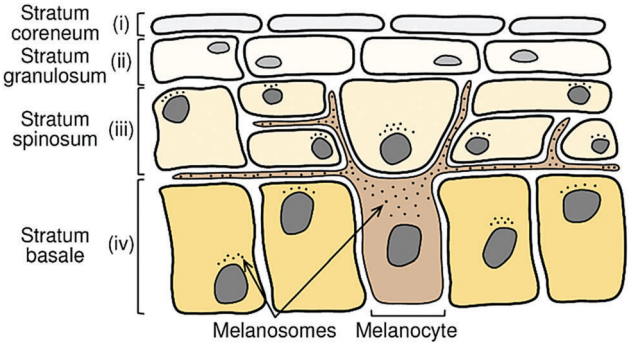

Fig. 3 Schematic representation of the upper epidermal layers of the skin. Melanocytes in the stratum basale layer extend out to surrounding keratinocytes in the stratum basale and spinosum layers. Melanocytes synthesise melanin-containing melanosomes which are transferred to the surrounding keratinocytes. The melanosomes form a supranuclear cap above the nucleus of the host keratinocyte, in the path of incoming UVR. This figure is adapted from ref. 24.

thence to surrounding keratinocytes.[32,33] Once the melanosomes are inside their host keratinocyte, they are positioned around the nucleus forming a supranuclear cap in the path of incident UVR. The overall photoprotection provided will depend on the concentration and distribution of melanocytes, and their size and morphology, as well as the concentration of melanin inside the melanosomes – properties which are regulated by a set of genes *via* processes collectively known as melanogenesis.[25,30,34]

Melanogenesis turns a static picture of photoprotection into a dynamic, adaptive, photoprotective process. For example, when skin is subjected to high levels of UVR, against which the current level of skin pigmentation offers insufficient protection, signalling pathways up-regulate melanogenesis, thereby increasing the number of melanocytes and melanosome production, causing facultative skin colour (tanning).[35] Melanogenesis thus enables the body to respond to changing levels of UVR as well as metabolic requirements, which helps to maintain an adventitious position within the burden of disease (Fig. 1). Whether natural sunscreens are fully optimised remains a moot point, however. For example, we note recent work highlighting the phototoxic properties of melanin.[36] As such, the optimal position in the burden of disease may be a fine balance between photoprotection *versus* phototoxicity.

Plants have an analogous burden of disease relationship with UVR, as was also shown in Fig. 1. Exposure to too much UVR can, for example, damage vital photosynthetic machinery and thus reduce the efficacy of photosynthesis, whilst too little UVR (particularly UV-B) can render a plant more susceptible to invading pathogens and reduce the UV-B signal transduction pathways that underpin many physiological processes.[38,39] Plants often employ sinapate ester derivatives as chemical filters to protect against overexposure to UVR. For example, sinapoyl malate (shown in Fig. 2) has been identified as such a sunscreen molecule in thale cress (*Arabidopsis thaliana*).[40,41] In this case, the phenylpropanoid pathway is the gene regulated response to changing levels of UVR. When overexposed to UVR, the phenylpropanoid pathway can be up-regulated to synthesise more metabolites – *e.g.* sinapate esters like sinapoyl malate – and deposit them in the vacuoles of the upper epidermis, thereby increasing UVR protection for sensitive cells in lower layers of the plant leaf.

The foregoing serves as a brief overview of some of the natural photoprotective responses prevailing in both humans and plants to changing levels of UVR. There remains an obvious issue, however: the response is not immediate. Immediate tanning actually provides little additional photoprotection, since it involves oxidation of pre-existing melanin. Additional photoprotection develops over 3 days or more,[42,43] by which time photodamage may well already have occurred. Further, given the recent growth in travel and tourism, as well as current cosmetic trends in tanning,[43,44] people are increasingly becoming exposed to UVR environments against which their skin is not protected – necessitating additional photoprotection *via* other means.

Artificial photoprotection

Fortunately, there are many ways by which one can reduce the potentially damaging effects of UVR.[45–47] Environmental factors – *e.g.* time of day, season, latitude, altitude and the terrestrial environment – all influence the local intensity of UVR. Clearly, avoiding high-UVR environments, or preparing for them appropriately by, for example, taking shade, wearing appropriate clothing, or using sun glasses, will substantially reduce the likelihood of UVR damage.

Whilst such behaviours will obviously help mitigate against damage from UVR, there remains a demand for additional photoprotection – not least because we want to sunbathe. Sunscreen products are the almost universally accepted 'solution'. These are applied to the upper epidermis of the skin and serve to complement the natural photoprotection provided by skin pigmentation. They contain components which are responsible for intercepting UVR and dissipating the energy through safe processes.

These components typically partition into two classes: chemical filters and inorganic particulate filters.[13,48,49] Chemical filters (sometimes referred to as organic filters) are typically aromatic molecules with a high degree of charge conjugation. They display intense, broad absorptions across the UV-A and/or UV-B regions, typically associated with $\pi^* \leftarrow \pi$ electronic transitions. Following photoexcitation, an effective chemical filter molecule will dissipate the absorbed energy as heat to its immediate surroundings, *via* one or more non-destructive pathways[24] of the types described later in this Review. The inorganic filters used in commercial sunscreens are typically nanosized particles that, again, display broad absorption across the UV-A/B wavelength range. These particulates also scatter incoming radiation away from the skin; indeed, they are sometimes termed inorganic scatterers. The relative efficiencies of absorption and scattering depends on the particle properties (*e.g.* diameter, surface coating, *etc.*).[50]

Appropriate combinations of chemical and inorganic particulate filters can obviously provide the broad spectral coverage that serves as one of the defining properties of any good sunscreen product. However, there are several other important considerations when designing a commercial sunscreen product: the

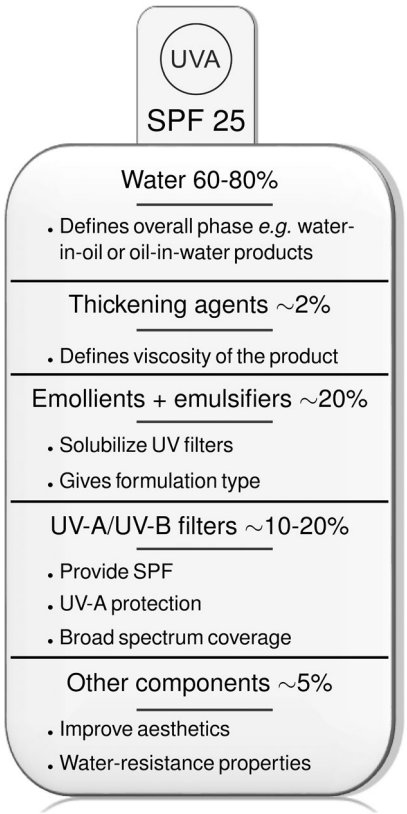

Fig. 4 The typical formulation of commercial sunscreen products.[37] The European symbol of UV-A protection is shown. SPF defines the sun protection factor, a laboratory measure of the fraction of sun burning radiation that reaches the skin, *e.g.* an SPF of 25 means 1/25th of the radiation reaches the skin if a layer of 2 mg cm^{-2} sunscreen is applied, compared to skin with no sunscreen use.

texture, ease of application, degree of water-resistance, required frequency of application, suitability for a broad range of skin types and conditions, odour, and production costs all need to be factored in when designing the product. As such, a typical sunscreen product contains many ingredients for reasons other than simply providing protection from UVR, as shown in Fig. 4. Beyond these design criteria, there are further physiological requirements. It must be safe to apply the product to the skin. No harmful components must be absorbed into the blood stream. Such concerns are central to the aforementioned 'sunscreen controversy': incidences of skin cancer continue to rise,[51] but there are also a growing number of studies that flag concerns regarding some of the commonly used filters.[14,15,52–54]

2. Requirements of a chemical filter

A basic photochemical perspective

The molecular constituents present within natural or commercial sunscreens are required to dissipate the absorbed photon energy efficiently and, as best as possible, without detriment to their integrity. Photoexcitation is viewed as the instantaneous promotion of an electron from one orbital to a higher energy orbital, resulting in an excited state (henceforth labelled S_1) with an electronic configuration different from that of the ground state (S_0). The excited state molecule will have a finite (short) lifetime before decaying. The mechanism of this decay is typically dependent on the molecule, the excitation energy, and the environment. Many of these possible decay mechanisms were first systematised by Jablonski, in the form of a diagram that still carries his name.[55,56] This distinguishes radiative and non-radiative decay processes. Radiative decay between states of the same spin multiplicity is called fluorescence. The rate constant for the $S_1 \rightarrow S_0$ fluorescence decay process is directly related to the strength of the corresponding $S_1 \leftarrow S_0$ absorption. Non-radiative decay processes recognised in a traditional Jablonski diagram include internal conversion (IC, *i.e.* an energy conserving transfer of population between states of the same spin multiplicity) and intersystem crossing (ISC, whereby population transfers to a state of different multiplicity, *e.g.* $S_1 \rightsquigarrow T_1$, where T_1 represents the lowest energy state of triplet spin multiplicity). Other possible non-radiative decay processes include 'reaction', *e.g.* isomerisation, bond fission, *etc.* (which will often be energetically feasible when exciting a molecule at near UV wavelengths) and, in solution, collisional quenching and even bimolecular reaction. The particular photophysical properties required of a chemical filter for potential use as a sunscreen are (i) a large absorption cross-section in the UV-A/B region, together with (ii) a high (ideally 100%) probability for the resulting excited state population to decay by IC to the S_0 state, followed by (iii) relaxation to the original ground state geometry (*i.e.* minimal permanent conversion to another isomer).

Though informative, the traditional Jablonski diagram does not advise on the relative probabilities of the various decay mechanisms or on the eventual outcomes. Nowadays, a much clearer picture of the excited state dynamics can be obtained by monitoring the way in which the energy of a molecule changes as a function of variations in the nuclear geometry. Analogous calculations for ground state molecules can be traced back to the early days of quantum mechanics and the introduction of the Born–Oppenheimer approximation (the assumed separation of the electronic and nuclear contributions to the total energy of a molecule), and underpin traditional concepts like a reaction path from reactants to products proceeding through a transition state. Several of the figures later in this review show such potential energy curves (PECs), though these too are clearly over-simplifications. $3N$-6 coordinates are required to describe fully the nuclear motions in a non-linear N-atom molecule, and a full description of the evolution from reactants to products thus requires a suitably multi-dimensional potential energy or free energy surface.

An excited state formed upon photoexcitation has a different electronic configuration to that of the ground state molecule, and the ways in which the energy of any particular excited state varies with changes in nuclear geometry will generally be different to that of other excited states and of the ground state. Given the different topographies of the ground and excited state potential energy surfaces (PESs), there will often be regions of configuration space where the energy difference between

different electronic states becomes small or zero. Such points of degeneracy often constitute so-called conical intersections (CIs).

A full discussion of CIs is outside the scope of this review. Detailed descriptions can be found elsewhere.[57–60] For current purposes, it suffices to recognise that CIs between PESs are ubiquitous in polyatomic molecules and that these are now recognised as pivotal in defining photochemically-driven phenomena, including (ultrafast) IC processes by which excited state population is channelled back to the S_0 state in molecules defined as being photostable. Passage through a CI is termed non-adiabatic, since the instantaneous switch from one (adiabatic) PES to another involves intimate coupling between the electronic and nuclear degrees of freedom (which are otherwise viewed as separable within the Born–Oppenheimer approximation).

The probability of transition through a given CI depends on the strength of the coupling between the states involved in creating the CI. The reactive coordinate that drives a molecule towards a given CI contains components of one or more of the $3N$-6 normal mode eigenvectors along which the potential gradient towards the CI is favourable. The dominant eigenvector of this nuclear coordinate is generally termed the gradient difference (g) vector. At the point of degeneracy, another normal mode is required to enhance the coupling between the electronic states in order to permit the radiationless transition. This derivative coupling vector (h) is orthogonal to the g vector. Put simply, small motions along the h dimension facilitate the change in electronic configuration and thus electronic state. The g and h vectors are the dimensions along which the double-cone topography of the CI exists. The remaining $3N$-8 degrees of freedom belong to the seam space and do not promote electronic state changes at small nuclear displacements. Various geometries and types of CIs are possible. Their geometric positions are often dictated by symmetry but can also be altogether accidental in larger and more complex polyatomic molecules. We revisit some of these ideas when discussing specific examples in the next section.

Mechanisms of photostability

Here we describe several generic types of CI geometry that are known to facilitate the IC of excited state population to the ground state. In each case, we start with a simple 'prototype' molecule, and describe the ways in which a specific mechanism extrapolates and changes with increasing molecular complexity.

Any energetically accessible CI between the excited and ground state PESs can facilitate non-radiative transfer of excited (*e.g.* S_1) state population back to the S_0 state and thus potentially reform the starting parent molecule. The probability of any such route to molecular photostability depends on several factors: (i) the topography of the excited state PES connecting the Franck–Condon region (*i.e.* the geometry with which the excited state molecule is 'born' upon photoexcitation from the S_0 state) to the CI geometry, (ii) the topography of the ground state PES between this CI geometry and the S_0 minimum energy geometry, and (iii) the vectors associated with the nuclear kinetic energy along a particular driving coordinate – the components of which largely depend on the potential gradients experienced prior to and following IC through the CI. Local environments that surround a given molecule (such as solvation) can influence the PES and thus the vectors associated with the nuclear kinetic energies. The overall dynamics in the presence of proximal solvent molecules will also be influenced by classical processes like thermal energy transfer and collisional deactivation.[61,62]

The first decay mechanism we consider is photodissociation, a primary process that runs counter to the requirements for photostability. Photodissociation is the fragmentation of a molecule following photon absorption, which we first illustrate by reference to water.[63–67] The valence orbitals of water can be pictured as two O–H centred σ orbitals, the two corresponding O–H centred antibonding σ* orbitals and a $2p_x$ lone pair orbital perpendicular to the molecular plane. Considering just these orbitals and without invoking symmetry, the ground state electronic configuration of water is: $(\sigma)^2(\sigma)^2(2p_x)^2(\sigma^*)^0(\sigma^*)^0$. Photoexcitation promotes an electron from the highest occupied $2p_x$ orbital to one of the σ* orbitals, yielding a ^{1}nσ* excited state with configuration $(\sigma)^2(\sigma)^2(2p_x)^1(\sigma^*)^1(\sigma^*)^0$ and $^1\Pi$ term symbol (at linear geometry). Electronic excitation weakens one of the O–H bonds, to the extent that the excited state PES is dissociative with respect to extension of one O–H bond, yielding H + OH radicals. As Fig. 5(a) shows, the ground and excited state potentials intersect in this coordinate at linear geometries (*i.e.* H–O–H bond angle = 180°). Motion along the bending coordinate (*i.e.* along the h vector) lifts the degeneracy of the $^1\Pi$ state, leads to the characteristic double cone topography of the symmetry allowed CI between the $^1\Pi$ (A′) and S_0(A′) states but has relatively little effect on the potential energy of the other $^1\Pi$ (A″) component (wherein the singly occupied p_x orbital is orthogonal to the nuclear plane). Other hydride molecules with similarly low lying, dissociative ^{1}nσ* states include methanol (forming CH_3O + H)[68–72] and higher alcohols, hydrogen sulphide (forming SH + H),[65,73] alkyl thiols, ammonia (forming NH_2 + H)[65,66,74] and alkyl amines.

Replacing one H atom in water with a phenyl group yields phenol, a molecule whose photodissociation dynamics have attracted much recent attention.[75–79] The presence of the π system (*cf.* H_2O) ensures that the first excited (*i.e.* S_1) state has $^1\pi\pi^*$ character. As Fig. 5(b) shows, this state is bound with respect to O–H bond elongation. The analogue of the ^{1}nσ* state of water is the S_2 state in phenol. This state is best viewed as having $^1\pi\sigma^*$ character, as the O($2p_x$) lone pair is stabilised (and thus lowered in energy) *via* conjugation with the π system. As in water, the $^1\pi\sigma^*$ state is dissociative with respect to O–H bond extension and crosses the S_0 potential at $R_{O-H} \sim 2$ Å, leading to a symmetry allowed $^1\pi\sigma^*/S_0$ CI – for which the h vector involves out-of-plane motion (notably O–H torsion). A second CI is also evident, between the $^1\pi\pi^*$ and $^1\pi\sigma^*$ states at smaller R_{O-H}. Experiments have shown that photoexcitation to both the S_1 and S_2 states of phenol results in O–H bond fission. The latter is unsurprising, and driven by direct dissociation. The former involves initial tunnelling from the $^1\pi\pi^*$ state to the $^1\pi\sigma^*$ state, through the barrier created by the $^1\pi\pi^*/^1\pi\sigma^*$ CI, and subsequent bond extension on the $^1\pi\sigma^*$ PES.[80]

Photodissociation acts counter to the requirements of photostability, and reversing the ballistic motion in the case

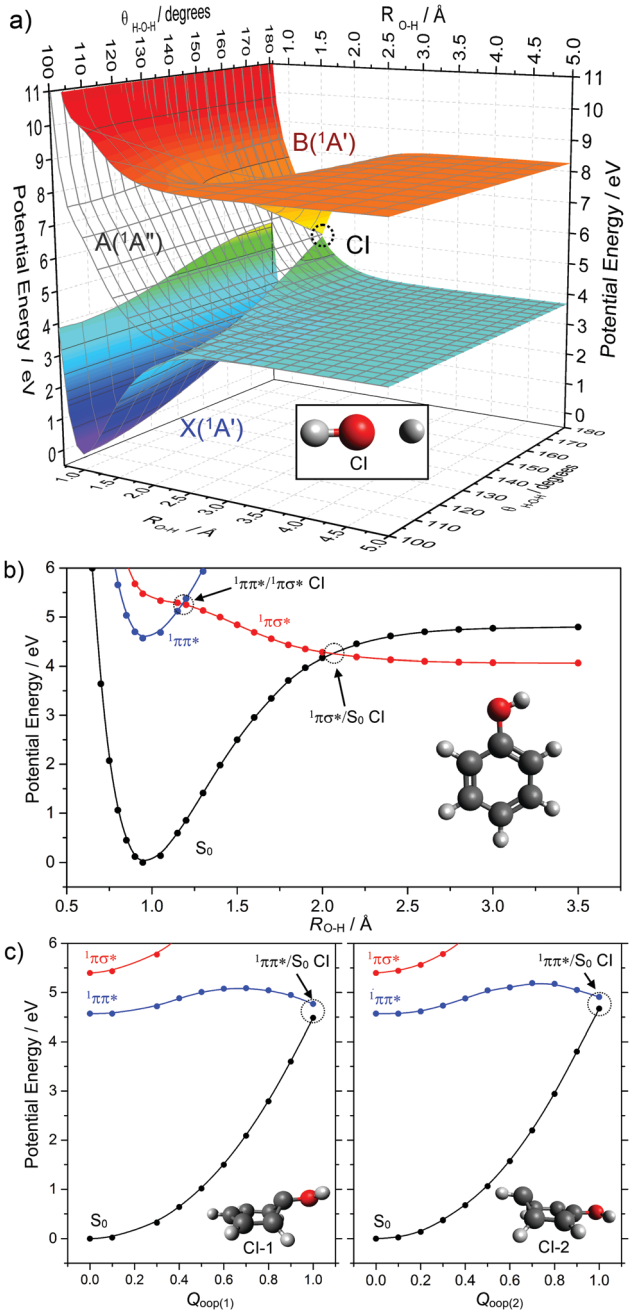

Fig. 5 (a) Potential energy surfaces of the ground ($X(^1A')$) and lowest singlet excited states ($A(^1A'')$ and $B(^1A')$) of water computed along the O–H stretch (R_{O-H}) and H–O–H bending (θ_{H-O-H}) coordinates. The CI at a linear geometry is clearly identifiable at an extended O–H bond distance ($R_{O-H} \sim 1.5$ Å). (b) Potential energy curves for the ground and lowest singlet excited states ($^1\pi\pi^*$ and $^1\pi\sigma^*$) for phenol along R_{O-H}. (c) Potential energy curves for these same three singlet states of phenol along two out-of-plane (oop) ring deformation coordinates ($Q_{oop(1)}$ and $Q_{oop(2)}$). The corresponding $^1\pi\pi^*/S_0$ CIs are indicated by the grey circles with the relevant optimised geometries at each CI shown in each panel.

of a light, fast, departing H atom is improbable. But Fig. 5 serves to illustrate a much wider family of molecules where a CI along a bond extension coordinate could facilitate IC between an excited state and the ground state. Firstly, the local topography in the region of the CI is important in determining the relative probabilities of bond fission (photodamage) and IC (and thus potential photostability). Second, non-adiabatic coupling in the vicinity of the CI may well be greater in the case of heavier, more slowly separating leaving groups. Third, the foregoing discussion has implicitly assumed collision-free conditions, but a surrounding solvent cage can encourage geminate recombination, re-sampling of the CI region and another opportunity to access the S_0 potential.[81]

Even a molecule as small as phenol has sufficiently high dimensionality to ensure the existence of many other CIs between the S_1 and S_0 PESs (and between other excited states), any of which could facilitate IC if the molecule has sufficient internal energy to sample the relevant regions of configuration space. Many of these alternative CI geometries can be pictured more easily in the context of phenol's close brother: benzene.[57] Fig. 5(c) provides schematic depictions of two out-of-plane (oop) ring deformations in phenol that are representative CI geometries in many conjugated cyclic systems.

Motion towards such CIs in the specific case of phenol is hampered by a potential barrier between the Franck–Condon and CI geometries. But CIs with oop ring puckered geometries are known to facilitate the ultrafast IC of excited state population back to the S_0 state (ultimately leading to photostability) in many larger and more complex molecules. Notable examples include the DNA and RNA nucleobases,[82–84] for each of which the potential energy profile linking the Franck–Condon region and at least one CI with an oop ring puckered geometry is barrierless. This quite striking difference in the relative importance of oop CIs in enabling IC in phenol and in the nucleobases can be traced to a combination of effects arising from incorporating N atoms in the ring and substituent effects.[85]

These oop ring deformation CIs can be viewed as extensions of another well-known class of CI found in alkenes. Ethene,[86] for example, shows a CI between its S_1 and S_0 PESs upon rotation about the C=C double bond. Analogues of this CI enable the well-known $E \rightarrow Z$ photoisomerism intrinsic to all aliphatic alkenes, and such $E \rightarrow Z$ CIs are known to dominate the ultrafast excited state dynamics of many biologically and industrially relevant molecules.[87] An equivalent twist about a C=C bond in a cyclic aromatic system like benzene inevitably leads to the oop ring-deformation CI. Hence the frequent reference to oop ring deformation CIs in aromatic systems as 'ethylenic' CIs.[88]

The final classes of CI geometry considered here are those arising *via* proton-transfer (PT) reactions. These can occur within or between molecules, yielding intra-[89–91] and intermolecular PT,[92–94] respectively. Regardless of this distinction, all PT reactions require an acidic proton donor (DH) and a basic acceptor (A), and are known to facilitate excited state/ground state curve-crossings in hydrogen-bonded complexes (*i.e.* DH–A) as depicted in Fig. 6. These are commonly termed proton coupled electron transfer (PCET) reactions. Photoinduced PCET in a hydrogen-bonded complex starts with promotion of an electron from an acidic donor (D) orbital to an unoccupied orbital localised on the basic acceptor (A). This creates a $D^+H–A^-$

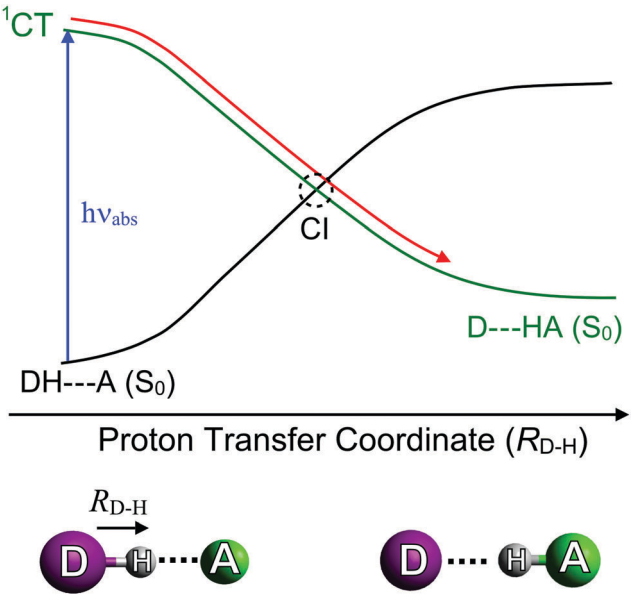

Fig. 6 Potential energy curves illustrating the variation in energy of the ground (S_0) state and a charge transfer (^{1}CT) state as a function of the proton transfer coordinate (R_{D-H}).

charge-separated or charge-transfer (CT) excited state, which is neutralised by the transfer of proton from D to A. A CT excited state almost always involves a favourable driving force for PT (*i.e.* a decrease in potential energy upon PT). The S_0 state, in contrast, is stable in the closed-shell DH–A configuration, and its PES exhibits a large potential barrier to PT. Inevitably, therefore, the CT and S_0 PESs cross along the PT coordinate and, as Fig. 6 shows, non-adiabatic coupling at the resulting CI could lead to formation of the D–HA adduct and/or reformation of the original DH–A pair. These limiting pathways can be viewed as photoreactivity and photostability, respectively.

3. Overview of experimental and theoretical methods

Experimental methods

Here we focus on contemporary methods designed to shed light on the early time dynamics that determine the efficacy (or otherwise) of a given chemical filter in a photoprotective role. A number of spectroscopic techniques have been used to probe the ultrafast excited state dynamics of such molecules in the gas-phase. These include both frequency- and time-domain methods. We choose not to discuss the former, but readily acknowledge the important role of such studies in revealing the energetics of relaxation processes and the vibrations that may facilitate these non-radiative decay pathways in related biomolecules; further discussion of such studies can be found in the literature.[95–101] Studies in the solution-phase are somewhat closer to real life applications. Both absorption and fluorescence techniques can be applicable. Here we focus on absorption-based techniques, but recognise that fluorescence probe methods can offer advantage on occasion. Finally, we must emphasise that 'more traditional', steady-state methods (UV/Vis absorption, NMR spectroscopies, *etc.*) have provided, and continue to offer, many important and complementary insights into dynamical processes occurring on longer timescales, which may lead to photoproduct formation.

The gas-phase; time-resolved mass-spectroscopy. Time-resolved mass-spectroscopy (TR-MS) experiments employ a skimmed molecular beam of the molecule of interest, generated by seeding its vapour pressure in a buffer gas, typically He or Ar. The gas is admitted into vacuum using a pulsed valve, and intercepted by femtosecond pump and probe laser pulses in the centre of an interaction region bounded by a carefully designed set of ion optics as illustrated in Fig. 7. UV photoexcitation by the pump pulse defines the start ($\Delta t = 0$) of the photochemical and photophysical processes that ensue. The probe pulse, delayed in time relative to the pump pulse, then ionises species (*e.g.* excited state parent molecules, photoproducts, *etc.*) within the beam. Given appropriate voltages on the different electrodes within the ion optics assembly, the resulting ions will be accelerated out of the interaction region, pass through a drift region, and eventually impact on a time and position sensitive detector. The ions entering the drift tube all have the same kinetic energy, but their respective velocities vary according to their mass-to-charge (m/z) ratios. Ions with different masses thus separate along the flight axis: lighter fragment ions reach the detector before heavier fragment ions and the parent ions, and a mass spectrum can thus be obtained.

The dynamical behaviour of the photoexcited molecule is revealed by monitoring how the yield of particular ion masses vary with the time delay between the pump and probe pulses (Δt).[102,103] Such parent and/or fragment ion transients can then be modelled using appropriate functions (*e.g.* exponential rise and decay functions) to describe the observed kinetics. These kinetic analyses yield time-constants that can be related to the underlying photochemical and photophysical processes in operation.

The solution-phase; transient absorption spectroscopy. A widely-used technique for probing the excited state dynamics of a target molecule in solution is transient absorption spectroscopy,

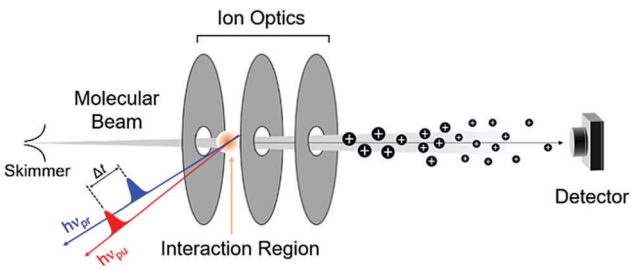

Fig. 7 Key features of a typical gas-phase experiment, including a molecular beam and a time of flight (TOF) mass spectrometer. The molecular beam is intercepted by the pump, $h\nu_{pu}$, and probe, $h\nu_{pr}$, laser pulses, which are represented, respectively, by the red and blue arrows. A suitably biased set of ion optics accelerates the ions formed by the probe laser towards a detector. The last section of such an apparatus consists of a field-free flight tube (see main text), so that ions reach the detector at different times depending on their m/z ratio. Figure adapted from ref. 95.

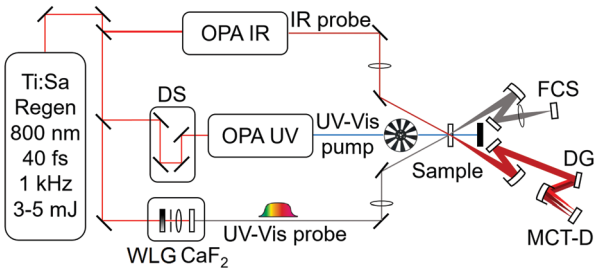

Fig. 8 Schematic showing a typical 'combined' experimental set-up for transient electronic absorption and transient vibrational absorption spectroscopy (TEAS and TVAS, respectively). The experiment employs OPAs seeded by the output of a Ti:sapphire regenerative amplifier laser. Other components shown include: white light supercontinuum generation (WLG) in a CaF_2 disk; delay stage (DS); dispersion grating (DG); mercury cadmium telluride detector (MCT-D); and fibre couple spectrometer (FCS).

wherein the change in absorption of a photoexcited molecular ensemble is tracked as a function of pump–probe time delay. This technique employs a flowing sample of the molecule of interest dissolved in an appropriate solvent. $\Delta t = 0$ is defined by a UV pump pulse that initiates the photophysics, which are then monitored *via* the transmission of a time-delayed probe pulse through the photoexcited region of the flowing sample. In most contemporary experiments, the probe pulse spans a broad range of wavelengths and is spectrally dispersed after passage through the sample using a spectrometer. Standard set-ups employ a broad-band white light continuum (WLC) – to monitor the UV/vis (electronic) spectrum[104–106] – or an optical parametric amplifier (OPA) operating in the infrared (IR) to monitor selected regions of the (vibrational) spectrum,[107–109] as illustrated in Fig. 8. A mechanical chopper, operating at half the repetition rate of the laser, is typically placed in the path of the pump beam, thereby ensuring that the probe pulse samples alternating 'pumped' and 'unpumped' molecular ensembles. Thus, one can determine the (wavelength dependent) change in absorbance, usually reported as ΔOD (optical density), as a function of Δt. Such transient spectra can display a range of characteristic signatures attributable to, for example, a ground state bleach (GSB), an excited state absorption (ESA), stimulated emission (SE) and photoproduct absorption.

A good sunscreen filter should display a particularly simple transient spectrum. Oxybenzone (OB, a chemical filter featured as one of our case studies in Section 4) comes close to this ideal, as illustrated by Fig. 9, which shows transient UV/vis and IR absorption data obtained following 325 nm photoexcitation of OB in solution in cyclohexane.[110] The former spectrum is dominated by an ESA feature that peaks ~366 nm but spans almost all of the wavelength range accessible with the available WLC and exhibits an ultrafast decay (characterised by fs and ps time constants, the interpretation of which is discussed in Section 4). The transient IR spectrum is dominated by a GSB feature at ~1620 cm^{-1}, the bulk of which recovers with a ~8 ps time constant. This latter time constant is largely determined by the rate at which photoexcited species relax by transferring vibrational energy to the surrounding solvent molecules and

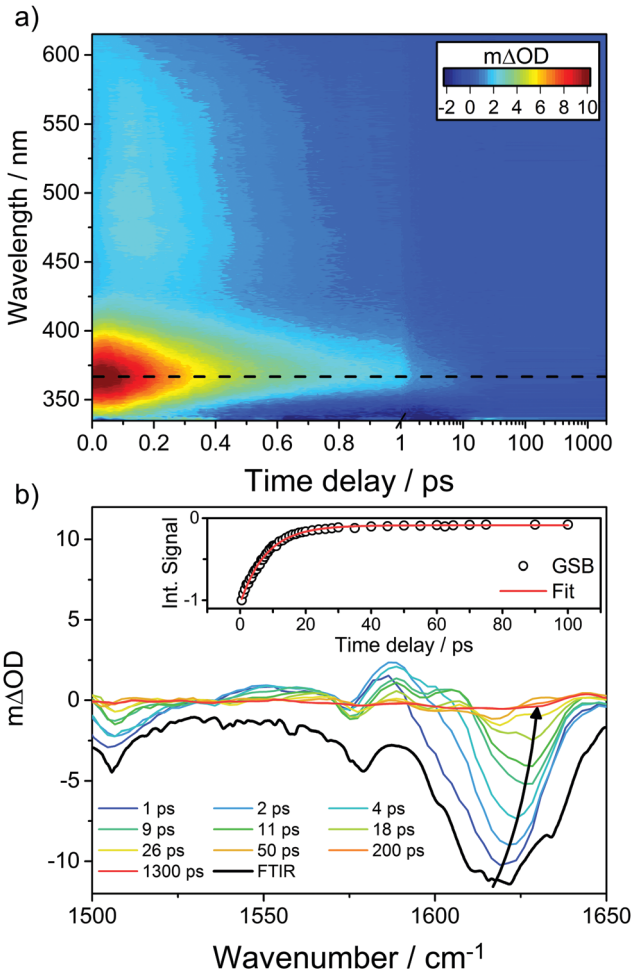

Fig. 9 (a) False colour plot showing the transient electronic spectrum (ΔOD as a function of probe wavelength and pump–probe time delay) following 325 nm photoexcitation of OB in cyclohexane, with the decay of the transient ESA signal centred at ~366 nm, represented by the black dashed line. (b) Transient IR spectra measured at different pump–probe delays (specified in the inset) in the range 1500–1650 cm^{-1} following 325 nm photoexcitation of OB in cyclohexane along with the steady-state Fourier transform IR spectrum of the precursor solution (shown by the bolder black line). The inset kinetic trace shows the best exponential fit to the integrated GSB signal (centred on ~1620 cm^{-1}, which blueshifts for larger pump–probe time delays as shown by the solid arrow) recovery. The original data are taken from ref. 110.

thereby repopulate the starting level of the S_0 state. (No similar GSB signal is evident in Fig. 9(a) simply because the electronic absorption spectrum of OB in its S_0 state barely extends to 340 nm, the short wavelength limit of the WLC probe.) Kinetic information is derived by modelling such transient absorption spectra recorded at many different pump–probe time delays using global fitting techniques.[111–114]

We re-emphasise that several other techniques can provide dynamical insights complementary to those revealed by TR-MS and/or transient absorption spectroscopies. In the gas-phase, for example, time-resolved velocity map imaging methods allow one to track photofragment and/or photoelectron velocity distributions, the analysis of which offers a route to untangling

at least some of the various relaxation pathways.[115,116] In the solution-phase, time-resolved fluorescence utilising optical Kerr gating,[117,118] and frequency up-conversion[119,120] or stimulated Raman scattering[121] methods could all provide insights complementary to those revealed by the transient absorption methods outlined above, but have yet to be applied decisively to studies of the kinds of chemical filters used in sunscreens.

We also emphasise that steady state measurements have long been used to explore photophysical properties of many sunscreen components, individually and in mixtures. Differences in the UV/vis absorption spectra of samples illuminated using, for example, an arc lamp and non-illuminated samples can provide information on photochemical stability, unwanted photoinduced production of singlet oxygen, and/or signatures of photodegradation products,[17,122] with NMR spectroscopy offering another route to product identification.[123] Such 'classical' photochemical studies have been crucial in the development of the many commercial sunscreens used today but are not discussed further since they do not report directly on the excited state photophysics that is the primary focus of this Review.

Computational and theoretical methods

Computational studies are equally necessary when it comes to any detailed description of likely IC mechanisms in the kinds of chemical filters used in sunscreens. Theoretical photochemists seek to determine (at least) approximate excitation energies, transition strengths and the likely dynamics along important nuclear coordinates, thereby offering an in-depth assessment of the feasibility of a given excited state reaction pathway. Existing computational methods are all challenged when it comes to calculating excited state energies, particularly in the regions of CI between electronic states that enable the ultrafast IC required for molecular photostability. The challenges stem from the multi-reference nature of CIs. The participating states (*e.g.* the S_0 and S_1 states) have comparable energies but different electronic configurations. The S_0 state wavefunction represents the lowest energy occupied orbitals in a single Slater determinant. Most methods use this determinant to construct a new set of reference ground state orbitals, which are then used to compute excitation energies.

However, the use of a single determinant reference configuration causes problems when states with different electronic configurations approach in energy. Multi-reference methods (such as CASSCF,[124,125] CASPT2,[126,127] MRCI[128]) circumvent this problem and have been used in many recent computational photochemical studies. Such calculations are expensive, however, and thus limited to relatively small molecular systems. Multi-reference calculations are not yet feasible for large systems, and we remain reliant on single-reference excited state methods (such as TD-DFT,[129,130] EOM-CCSD,[131] CC2[132] and ADC(2)[133]) which, when used with suitable caution, can provide valuable qualitative pictures of excited state decay processes.[134–137] These methods can be combined with classical theories in order to include environmental effects. Such calculations employ mixed quantum and classical (QM/MM) methods, where the chromophore is treated using high level electronic structure methods, while the surroundings (*e.g.* solvent molecules) are treated classically.[138–142]

The foregoing methods solve the time independent Schrödinger equation at selected nuclear geometries to determine the topography of the PES(s) for a given reaction path. They give no explicit information about the reaction dynamics. Timescales for an excited state reaction can be obtained by simulating the nuclear dynamics. Full quantum dynamics simulations, in which the nuclear degrees of freedom are tracked exactly by solving the time dependent Schrödinger equation (TDSE) represent the 'gold standard'. Such quantum dynamics calculations have traditionally been limited to PESs of reduced dimensionality on account of the computational expense. Simulations on multi- and full-dimensional PES(s) are starting to appear, but are currently restricted to very short ($\sim$100 fs) propagation times.

Much longer ($>$1 ps) timescales can be explored using semi-classical methods. Here, the electronic coordinates are computed by numerically integrating the TDSE (thereby retaining the possibility of non-adiabatic coupling between states), while the nuclear coordinates are driven classically by solving Newton's classical equations of motion. This is the premise behind Tully's fewest switches surface hopping (FSSH) algorithm,[143] that is now included in several QM packages.[144–146] FSSH can be used in combination with available PESs or can be programmed so that, at each time-step along the nuclear propagation, the energies and gradients of the various electronic states are computed 'on-the-fly' using a suitable QM or QM/MM electronic structure method(s).

Another important recent development has been the advent of the GPU-accelerated *ab initio* multiple spawning (AIMS) method for treating excited state dynamics. In AIMS, the nuclear dynamics and electronic structure problems are solved simultaneously, thereby allowing quantum behaviour (*e.g.* tunnelling) of the nuclei. GPU-accelerated AIMS has been successful in modelling the photoinduced ring-opening of an isolated molecule as large as provitamin D_3 (a 51 atom system)[147] and used to treat the excited state dynamics of a range of solvated chromophores.[148] It is safe to predict that GPU-accelerated dynamics methods will become increasingly popular and important for simulating photochemical process in complex environments.

4. Case studies

Molecular constituents in natural sunscreens

Natural sunscreen molecules play a key role in protecting the vital genetic material contained within an organism. Thus, they tend to be present nearer the surface of most organisms. Natural sunscreen molecules will also exhibit the fundamental photophysical properties identified in Section 2 – namely (i) a high absorption cross-section for incident UVR (typically satisfied by a conjugated π system) and (ii) one or more mechanisms whereby the absorbed photon energy can be dissipated without loss of molecular integrity. Here we summarise results from recent studies that seek to unravel dynamical details of

these dissipation mechanisms in both plant and mammalian sunscreens.

Plant sunscreens. Lignin is one of the most abundant naturally occurring biopolymers on Earth.[149] It provides structural support, water transport and protection against microorganisms in vascular plants.[149,150] The composition of lignin is species dependent, but all lignins, though species-dependent, are cross-linked phenolic polymers, mostly derived from three monolignols (*p*-coumaryl, coniferyl and sinapyl alcohols),[149,150] and all are highly photostable against exposure to UVR.

Efforts to understand the photostability of lignin include gas-phase studies of the excited state dynamics of phenol, guaiacol and syringol following photoexcitation to their respective $S_1(^1\pi\pi^*)$ states.[152,153] Fig. 10 compares these model chromophores (henceforth abbreviated as ArOH) with the relevant monolignols and a small section of lignin polymer. The measured quantities in this study were the respective S_1 state lifetimes and the H atom yields (attributed to ArO–H bond fission) measured at the longest available pump–probe time delay (Δt = 1.2 ns). On the basis that ArO radical formation drives photodegradation,[154] the relative photostabilities were found to be ordered: guaiacol > syringol > phenol. Intriguingly, this order matches that of the relative abundances of the monolignol building blocks in natural lignins,[155] which are often dominated by coniferyl alcohol (which shares the same aromatic motif as guaiacol) with little (<10%) of the simplest phenol-based analogue, *p*-coumaryl alcohol.

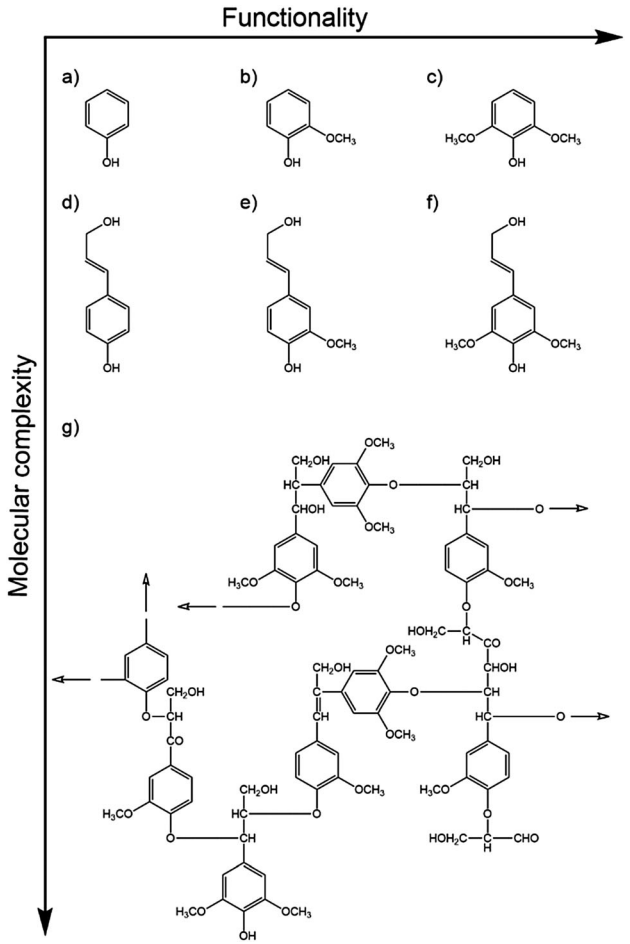

Fig. 10 Model chromophores of the cross-linked phenolic polymer lignin, with increasing functionalisation and molecular complexity. Phenol-based chromophores: (a) phenol, (b) guaiacol, (c) syringol, and the more complex monolignols: (d) *p*-coumaryl, (e) coniferyl and (f) sinapyl alcohol. These form the building blocks of beech lignin,[151] a subunit of which is shown in (g). Hollow arrows indicate the directions of further polymerisation.

The relative photostabilities of these model chromophores are seen to correlate with the extent of intramolecular hydrogen bonding. O–H bond fission in each case involves tunnelling through the potential barrier associated with the CI between the $^1\pi\pi^*$ and $^1\pi\sigma^*$ states (recall Fig. 5(b)), which offers greatest impediment at planar geometries. Excited state tunnelling probabilities are thus reduced if out-of-plane (torsional) motion of the O–H moiety is constrained by intramolecular H-bonding with the O atom in the one (in guaiacol) or two (in syringol) neighbouring $-OCH_3$ groups. The extent to which these gas-phase findings translate into the condensed phase remains an open question. Transient absorption studies show that the relative behaviours persist in a weakly interacting solvent like cyclohexane: ArO radicals were clearly visible within 1 ns when exciting phenol in cyclohexane[156] whereas, even at pump–probe delays Δt = 8 ns, it was hard to discern any ArO radical formation following UV photoexcitation of guaiacol in cyclohexane.[61] Thus it is tempting to speculate that such behaviour might extrapolate to nature, given that solvation (by H_2O) will be discouraged by the hydrophobic nature of the biopolymer (lignin).[154]

Sinapoyl malate was introduced earlier (Fig. 2) as a prominent example of a naturally occurring sunscreen molecule. It contains the syringol motif and is also a cinnamate derivative. Cinnamates are aromatic, unsaturated salts and esters derived from cinnamic acid – many of which have been studied both theoretically and experimentally.[157] Gas-phase UV spectroscopy studies of sinapoyl malate, sinapic acid, and other sinapate esters show that they all absorb strongly in the UV-B region. Unlike the others, however, the absorption spectrum of sinapoyl malate is broad and featureless, even under jet-cooled conditions.[158] In each case, the UV absorptions are attributed to $\pi^* \leftarrow \pi$ excitations, involving orbitals that are delocalised across the ring and the conjugated side-chain. IR-UV double resonance studies serve to exclude spectral congestion (*e.g.* from the presence of different conformers) as the cause of the apparently featureless absorption of sinapoyl malate. Rather, it is taken as evidence that the $^1\pi\pi^*$ state is short-lived, and couples efficiently with a near resonant, optically 'dark' excited state (*i.e.* another excited state with a very small absorption cross-section from the S_0 state). Evidence in support of this conjecture is provided by TD-DFT calculations, which suggest that the dark state is a $^1n\pi^*$ state with substantial charge-transfer character.[158]

The steady-state fluorescence spectrum following excitation of an aqueous solution of sinapoyl malate at its UV absorption maximum shows a large Stokes shift and a low fluorescence quantum yield, $\phi_{fl} \sim 3 \times 10^{-3}$ – suggesting that population in this $^1n\pi^*$ state also undergoes efficient non-radiative decay. Given the prior work on syringol, it is unlikely that the rate of

O–H bond fission could be sufficient to account for this decay. Further insights into the decay mechanism have been provided by ultrafast UV pump – UV/vis absorption probe studies of sinapoyl malate in a range of solvents (dioxane, acetonitrile and methanol),[17] which confirm that photoexcitation of the majority *E*-isomer at ~330 nm results in ultrafast deactivation. Global fitting the measured transient absorption spectra revealed three decay processes with respective time constants τ_1 (sub-ps), τ_2 (~1–5 ps) and τ_3 (~20–30 ps), the precise values of which are solvent dependent. Two possible relaxation mechanisms were proposed. Both assume initial photoexcitation to a strongly absorbing $1^1\pi\pi^*$ state. One assumes that the population evolves on the initially excited state, while the other assumes efficient non-adiabatic coupling to another excited state (*e.g.* the CT state suggested by Zwier and coworkers).[158] In either scenario, the excited molecule is assumed to distort – most plausibly (by analogy with the documented photophysics of other cinnamates) – along the *E*–*Z* isomerisation coordinate towards a region of CI with the S_0 PES. Vibrational energy transfer to the surrounding solvent cools the resulting S_0 molecules. In no case did the parent absorption spectrum recover fully within the maximum time delay available (Δt = 2 ns), suggesting that some S_0 molecules initially cool into the higher energy *Z*-isomer.

Though appealing, this description still leaves a lot of room for refinement. For example, recent excited state quantum dynamics calculations coupled with classical molecular dynamics (MD) simulations of the ultrafast non-radiative decay of sinapic acid – in isolation, and when microsolvated with methanol – offer additional insights into the early time excited state dynamics of this precursor to sinapoyl malate.[159] Specifically, these simulations suggest an important role for proton transfer, enabled both by intramolecular (in the case of the bare molecule) and intermolecular (in the complex with methanol) hydrogen bonds in the photoexcited molecule.

The latter finding, in particular, may help account for the solvent dependent excited state decay kinetics observed following UV photoexcitation of sinapoyl malate. Whilst some mechanistic details remain to be resolved, there is no question that sinapoyl malate undergoes ultrafast decay to regenerate (predominantly) the original ground state molecule – justifying its use as a photoprotective sunscreen in plant leaves. As noted earlier, lignins are ubiquitous in nature. Could it be that evolution has favoured constituents that offer a multiplicity of ultrafast excited state decay pathways, capable of functioning in a range of different environments? Sinapoyl malate is not used in commercial sunscreen products, but further studies of this and related naturally occurring systems will surely provide further insights into the design of new, and/or the optimisation of existing, sunscreens.

Mammalian sunscreens. The mammalian body contains many molecular components that act as UV filters and display the necessary photophysical properties, *i.e.* a conjugated π-system for effective UV absorption and fast non-radiative decay pathways that enable efficient reformation of the ground state parent molecule.

We start with arguably the most famous class of photostable biomolecular systems: the DNA/RNA nucleobases and nucleosides. Adenine, thymine, guanine, cytosine and uracil (and their nucleosides) are DNA/RNA constituents and carry the genetic code in all biotic systems. Their primary role is to code for and subsequently generate proteins that maintain biotic life. However, the structural properties of the DNA/RNA nucleobases, nucleobase pairs and nucleosides offer secondary benefits, including acting as a sunscreen and thus protecting genetic information stored within the cell. DNA/RNA nucleobases are known to undergo intrinsic ring-centred oop deformations following UV photoexcitation that mediate ultrafast IC and efficient reformation of the ground state parent molecule.[85,160–163] Such oop deformation-based IC routes are also intrinsic to the DNA/RNA base pairs and isolated nucleosides, but these can also undergo IC along PCET reaction paths – which are proposed to account for the much shorter excited state lifetimes of nucleosides compared to the isolated nucleobases.[85,135,164] Within the cellular medium, strands of RNA, ADP or ATP, that contain analogous molecular moieties to that of DNA nucleobases and nucleosides, are also expected to show some degree of photostability – protecting their molecular integrity and the local environment by absorbing (and thus reducing) the incident UV flux. Nucleobases and nucleosides are generally contained well within the cellular environment, however, and are only exposed in abnormally harsh and penetrating UV-environments.

Other molecular sunscreens exist nearer the surface of the mammalian body. Consider the eye, for example. Its primary function is to direct light to photoreceptors located on the retina called cones and rods. The latter contain the protein rhodopsin, which houses the chromophore retinal. Retinal is extremely photostable and has been the focus of many experimental and theoretical studies. Retinal, and its protonated Schiff base, are both known to undergo ultrafast IC *via* low energy CIs located along *Z*/*E* photoisomerism coordinates.[87,165–171]

The lens, which focuses light onto the retina, contains many molecular constituents that help protect it (and the surrounding environment) from hard UV radiation. Kynurenines (see inset of Fig. 11) are one such class of molecular constituents, which are biosynthesised by the tryptophan dioxygenase enzyme. Experimentally, kynurenines have been shown to undergo fast excited state decay following photoexcitation.[172] Theory suggests that the dominant mechanism in this case is IC *via* a CI located along a PCET coordinate as shown in Fig. 11.[134] Kynurenines contain acidic amino donor and basic carbonyl acceptor groups which, in at least some of the low energy conformations, are linked by strong intramolecular hydrogen bonds that facilitate the proton transfer.

The part of a human or mammal that is most exposed to light is the skin. Molecular sunscreens thus play their most significant roles on and in the skin. Sunscreens present on the epidermis manifest either *via* synthesis from skin cells (see Section 1) or in sweat. An example of the latter is urocanic acid (UA) which, as Fig. 12 shows, has some structural similarities to sinapic acid – with an imidazole ring in place of the substituted benzene. UA absorbs strongly in the UV and displays an

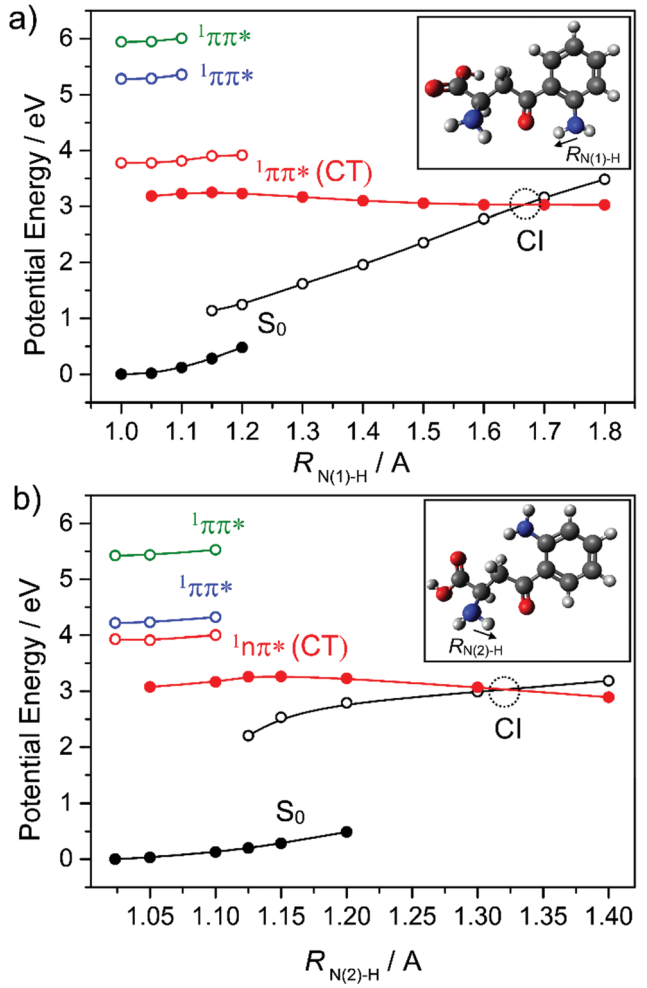

Fig. 11 Potential energy curves of the ground and first three singlet excited states of (a) *syn* and (b) *anti* kynurenine obtained by a constrained relaxed scan along the N–H bond elongation coordinates ($R_{N(1)-H}$ and $R_{N(2)-H}$) in the S_0 state (full black circles) and in the $^1n\pi^*$(CT) state (full red circles) – representing intramolecular proton transfer. The vertical excitation energies of the lowest $^1n\pi^*$ (empty red circles) and two $^1\pi\pi^*$ states (empty blue and green circles) from the relaxed S_0 geometries, and the vertical energies of the ground state (empty black circles) from the relaxed $^1n\pi^*$(CT) geometries are shown also. The data are taken from ref. 134.

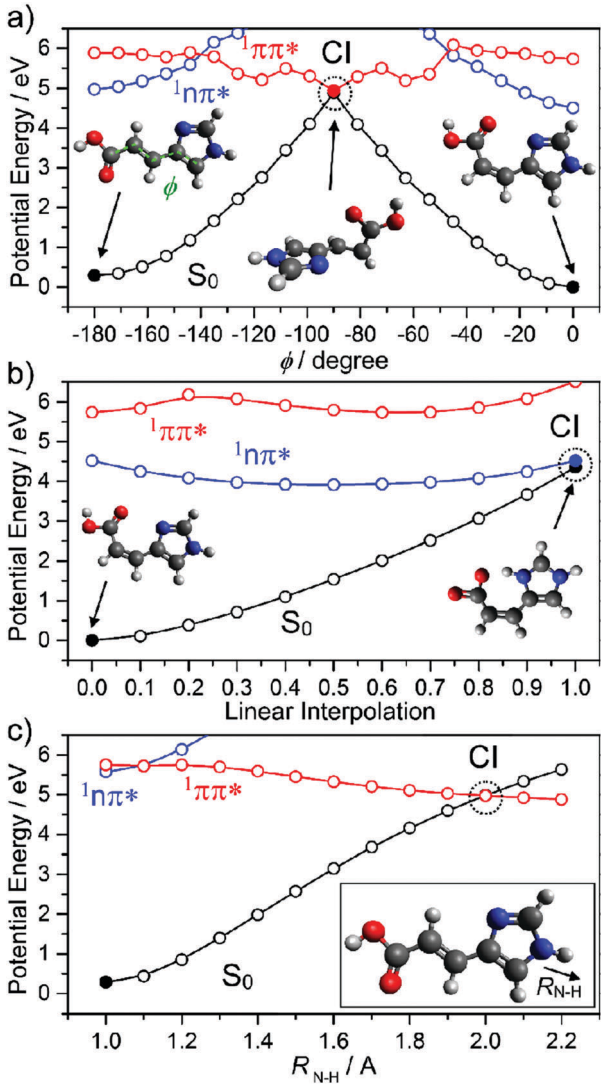

Fig. 12 Potential energy curves of the lowest three singlet states of urocanic acid as functions of (a) *E*/*Z* isomerism (φ), (b) the intramolecular proton transfer that may occur after *E*/*Z* isomerisation and (c) the potentially deleterious N–H bond fission (R_{N-H}). The data are taken from ref. 173.

ultrashort excited state lifetime in both the gas-phase and in aqueous solution. Electronic structure calculations and FSSH MD simulations identify the dominant relaxation path as IC *via* CIs located along an *E*/*Z* isomerism coordinate.[173,174] As Fig. 12(a) shows, population evolving through this CI can either reform UA in its global minimum ground state geometry (the *E* isomer) or branch into the minimum of the *Z* isomer. Both routes are thought to confer photostability, since the PE profiles suggest the reversible reformation of *E* or *Z* isomers by re-excitation.

However, we note an additional caveat. The lowest energy *Z* isomer has an intramolecular hydrogen bond between the OH (of the carboxylic acid group) and an acceptor N atom in the imidazole ring. This introduces another possible excited state decay path, PCET, which could drive reformation of the ground state parent molecule (and thus photostability). But it could also lead to formation of an imino product, which would likely act to reduce the efficacy of UA as a sunscreen. Recalling Section 2, we recognise $\pi\sigma^*$ state-mediated N–H bond fission as another possible (and potentially harmful) excited state decay pathway if UA is exposed to shorter (*i.e.* UV-C) wavelengths.

The final but arguably the most important class of natural sunscreen constituents considered here are epidermal based melanins. As outlined in Section 1, eumelanin and pheomelanin are ubiquitous in the human skin and contain structural elements that appear to be specifically adapted to filtering UVR. Eumelanin is a dark pigment, with common polymeric chains of cross-linked 5,6-dihydroxyindole (DHI), indole-5,6-dione, hydroxyindolone and 5,6-dihydroxyindole-2-carboxylic acid (DHICA) motifs (recall Fig. 2). The structure(s) of eumelanin are still under debate,[175] but oligomeric structures (shown in Fig. 13)

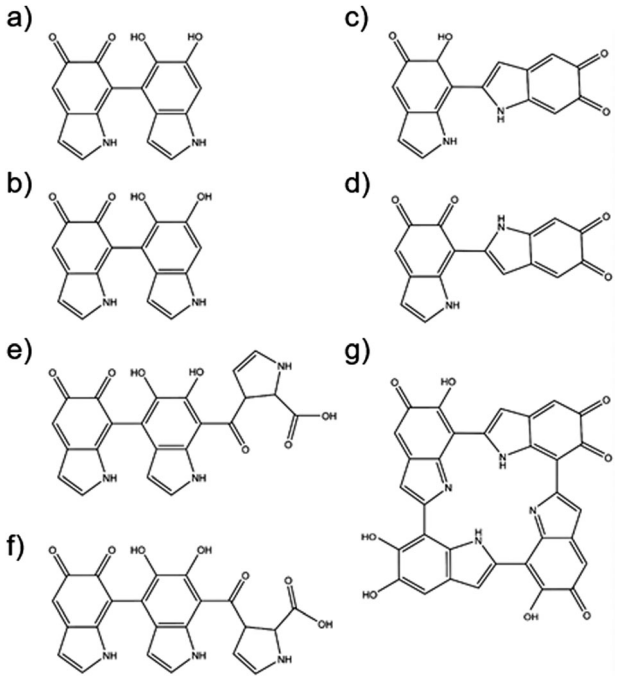

Fig. 13 Structures associated with various polymeric configurations of eumelanin.

are recognised with branched and π-stacked configurations. Many theoretical studies have sought to decompose and interpret the measured absorption profile in terms of weighted contributions from different plausible motifs.

Thus, for example, it is now concluded that absorption associated with oligomer chains containing fully hydrogenated DHIs lies in the near-UV, whereas that from partially (*i.e.* hydroxylindolone) or fully (*i.e.* indole-5,6-dione) dehydrogenated oligomers also contributes to the long wavelength tail of the measured absorption spectrum. Even the presence of just one non-fully hydrogenated form in the oligomer chain leads to a large bathochromic shift in the vertical excitation energy (*cf.* bare DHI).[175]

The excited state photophysics occurring following photoexcitation of small building blocks and/or oligomeric units present in melanins has been explored computationally and *via* solution-phase, ultrafast pump–probe studies.[157,176–179] Electronic structure calculations on DHI[180,181] suggest facile πσ*-state mediated O–H bond extension following $\pi^* \leftarrow \pi$ excitation (recall Section 2) which, in this case, has the net effect of migrating an H atom from the pendant OH to a neighbouring ring carbon atom. Photoprotection in this scenario is afforded primarily by the resulting isomeric species, 6-hydroxy-4-dihydro-indol-5-one, which is predicted to absorb strongly in the UV and visible spectral regions and to support excited states that undergo ultrafast IC to the S_0 state *via* a PCET mechanism.

Recent ultrafast pump–probe studies of DHICA and DHICA-derived oligomers offer another insight into the potentially complex modus operandi of natural sunscreen components.[182] These studies conclude that DHICA dimers are almost as efficient at dissipating UV-energy as the full polymeric pigment, and more than 1000-times more efficient in this role than the bare monomer – suggesting that the stellar photoprotective properties of black eumelanin pigments are a particular property of coupled DHICA units. Further, the authors identify two ultrafast excited state decay mechanisms (both intra- and intermolecular PT pathways) and find the dissipation rates to be relatively insensitive to the details of the sub-unit couplings.[182] Again, this deduced multiplicity of efficient decay pathways accords with the view that nature will have selected a particularly robust photoprotection strategy.

However, we end this section by reiterating the point that natural sunscreens are unlikely to be completely free of deleterious side effects. As noted earlier in this Review, melanin – known for its photoprotective properties – has recently also been shown to be potentially carcinogenic.[36] Similarly, the *Z*-isomer of urocanic acid has been observed to contribute to UV-induced skin cancer, likely through immunosuppression.[183,184]

Molecular constituents in commercial sunscreens

We now focus attention on chemical filters that find use in commercial sunscreen lotions designed to work alongside natural sunscreens and provide additional UV protection. Fig. 14 shows selected chemical filter molecules currently used in commercial sunscreens.[185] These broadly partition into seven classes, *i.e.* derivatives of: *para*-aminobenzoates; cinnamates; salicylates;

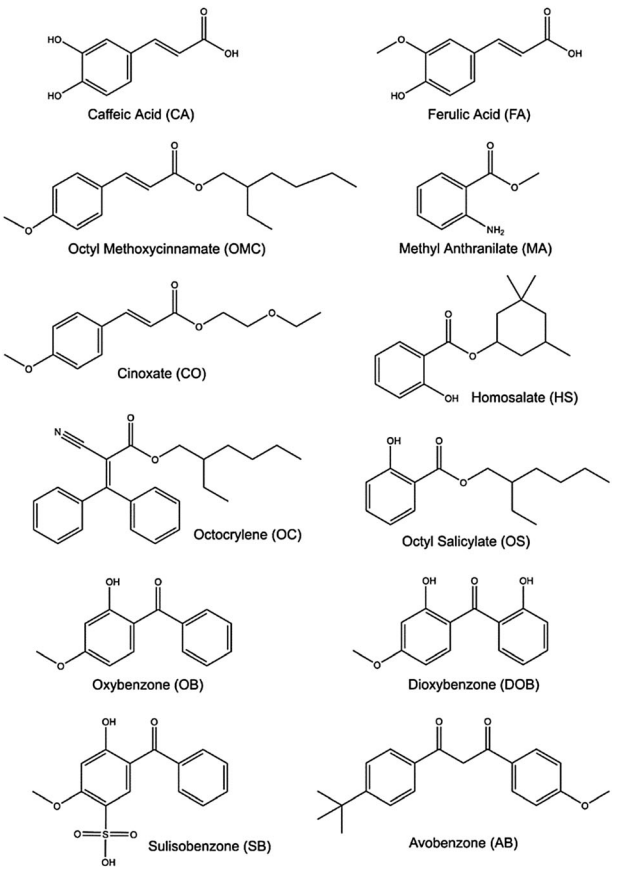

Fig. 14 Structures of some of the molecular constituents present in commercially available sunscreen products.

anthranilates; camphor; dibenzoyl methanes; and benzophenones. All bear at least some resemblance to components present in plant sunscreens.

Aromatic acids are the basis for several of these chemical filters, including caffeic acid (CA) and ferulic acid (FA). The latter finds greater use in commercial sunscreens, on account of its superior photostability.[186] Both can be viewed as substituted phenols and, as such, both could be prone to decay *via* $\pi\sigma^*$ state-mediated O–H bond fission following UV excitation. CA has two OH groups, only one of which can be 'protected' by an intramolecular H-bond, whereas the O–CH_3 bond is the pendant bond in the lowest energy conformer of FA. Analogy with prior (gas-phase) photofragmentation studies of phenol, anisole and catechol suggests that the free O–H bond in CA will be most susceptible to photodissociation.[187–189] Any such excited state bond fission will be in direct competition with non-radiative IC paths and thus reduce the photostability of CA. Several theoretical studies have addressed the strong near-UV absorption of FA,[190–193] while others have used highly correlated multi-reference methods to explore its possible excited state decay mechanisms.[191] These identify $E \rightarrow Z$ isomerism (Fig. 15), reminiscent of that prevailing in UA, as the dominant relaxation path following UV excitation of FA.

CA and FA can be viewed as building blocks for the more complex aromatic esters included in many commercial sunscreen products. Examples of such esters include octyl methoxycinnamate (OMC), cinoxate (CO), methyl anthranilate (MA), octocrylene (OC), homosalate (HS), and octyl salicylate (OS). As Fig. 14 shows, the structures of CO, OMC and OC have some analogies with FA and CA, and all contain aliphatic side-chains with conjugated C=C double bonds. Thus, it is reasonable to predict that similar *E*/*Z* isomerism pathways will contribute to the ultrafast decay of these species following absorption of UVR.

OMC is one of the most studied of these aromatic esters, and is chosen here as the first of three exemplars. Its excited state photophysics has been explored *via* both gas- and solution-phase experiments. Frequency-resolved gas-phase measurements reveal the existence of multiple rotamers.[194] Linewidth analysis implies a sub-ps lifetime for the $1^1\pi\pi^*$ excited state. However, TR-MS measurements using a 193 nm probe to ionise excited state molecules formed following UV excitation to the $1^1\pi\pi^*$ origin level returned an excited state lifetime of $\sim$20 ns.[194] These apparently contradictory findings were corroborated by later TR-MS studies with much higher pump–probe time resolution,[123] and confirmed the previously proposed operation of two photophysical processes: ultrafast non-adiabatic coupling from the 'bright' $1^1\pi\pi^*$ state to an optically 'dark' (in terms of absorption from the S_0 state) $^1n\pi^*$ state, which then decays on a much slower timescale. Such a mechanism is reminiscent of the excited state behaviour summarised earlier in the case of sinapoyl malate, and consistent with the deduced energetic ordering of the $^1\pi\pi^*$ and $^1n\pi^*$ excited states in several other cinnamate derivatives.[195–197] Neither TR-MS experiment used sufficiently energetic probe photons to confirm (or refute) the assumption that the slower decay provides a measure of the rate of $E \rightarrow Z$ isomerism required to couple population from the $^1n\pi^*$ state to the S_0 state. Such conclusions are also consistent with those advanced to explain TR-MS gas-phase results obtained for the simpler analogue, methyl-4-methoxycinnamate,[198] though a recent combined experimental and computational (TD-DFT) study has also argued the need for a triplet state pathway to reconcile the observed dynamics.[199]

Efforts to extend such measurements to the solution-phase include gas-phase microsolvation studies involving MMC.[194,197,198] TR-MS studies of MMC–H_2O clusters show that microsolvation accelerates the excited state relaxation. This has been explained by assuming that the proximity of the polar H_2O molecule destabilises the $^1n\pi^*$ state, thereby reducing (or even switching off) the coupling between the $^1\pi\pi^*$ and $^1n\pi^*$ states and allowing the rival $^1\pi\pi^* \rightsquigarrow S_0$ IC process (again mediated by $E \rightarrow Z$ isomerism) to be kinetically competitive.[196,198,200]

Solution-phase studies have led to similar conclusions. The NMR data shown in Fig. 16(a) confirms that steady-state UV illumination of the lower energy (*E*-) isomer of OMC in cyclohexane and methanol results in some conversion to the *Z*-isomer.[123] Fig. 16(b) shows that the molar extinction coefficient of *Z*-OMC in the UV-A/B spectral region is significantly smaller than that of *E*-OMC. Thus the observed decline in the peak absorbance of samples comprising initially pure *E*-OMC in cyclohexane or methanol upon prolonged exposure to UVR provides further (indirect) evidence for $E \rightarrow Z$ isomerism.[201] Time-resolved fluorescence measurements for both *E*-OMC and *Z*-OMC in cyclohexane solution returned excited state lifetimes $<$30 ps (the instrument response time).[201,202] These studies served to encourage higher time-resolution pump–probe transient electronic absorption measurements that provide further insights into the early time dynamics following photoexcitation at the wavelength of peak absorption (λ_{max}) of *E*-OMC, in both cyclohexane and in methanol.[123] Specifically, the *E*-OMC ($^1\pi\pi^*$) molecules prepared by photoexcitation are deduced to distort along the $E \rightarrow Z$ isomerisation coordinate and couple to a

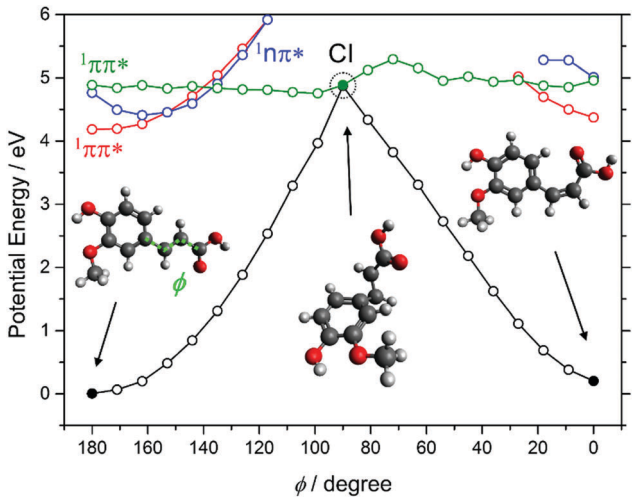

Fig. 15 Potential energy curves of the lowest four singlet states of ferulic acid computed along the *E*/*Z* isomerism coordinate (φ). The data are taken from ref. 191.

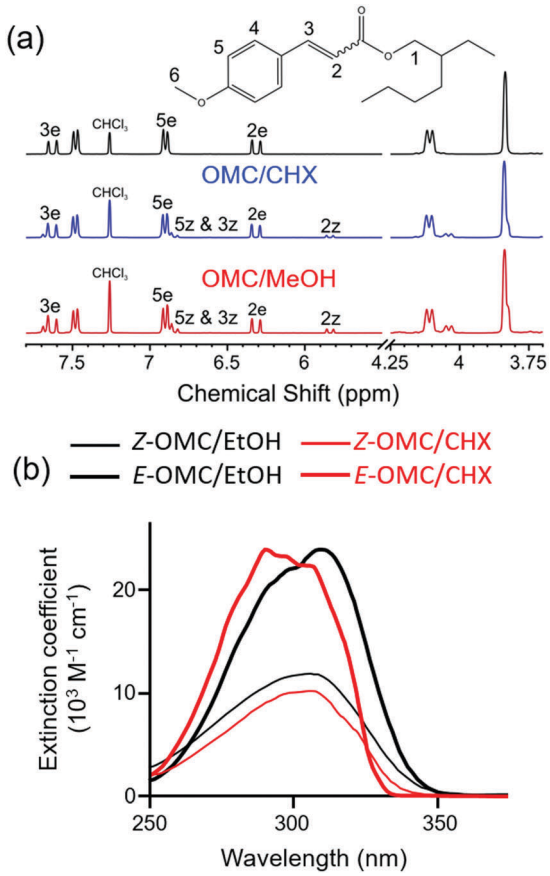

Fig. 16 (a) ^{1}H NMR spectra of *E*-OMC and peak assignments following irradiation at λ_{max} = 290 nm (CHX) and 316 nm (methanol). Adapted from ref. 123. (b) Absorption spectra of *E* and *Z* OMC in cyclohexane (CHX) and ethanol (EtOH). Adapted from ref. 201.

region of CI with the S_0 state with a 1–2 ps time constant; a much longer (>ns) transient feature was assigned to the long-lived *Z*-OMC isomer. Again, we note the obvious similarities between the excited state decay mechanisms deduced for this synthetic chemical filter and for the natural sunscreen sinapoyl malate.

Benzophenones are generally the most abundant synthetic chemical filters in commercial sunscreens. Examples include oxybenzone (OB), dioxybenzone (DOB), sulisobenzone (SB) and avobenzone (AB) – see Fig. 14 – the simplest of which is OB, our second exemplar, for which we showed transient absorption data in Section 3. Recent theory[191,203] and transient absorption experiments (exciting OB at 325 nm, in cyclohexane and in methanol solution)[110,204] both conclude that PCET, wherein the OH centred proton migrates to the carbonyl O atom (*i.e.* enol–keto tautomerism), represents the dominant relaxation path. Photoexcitation populates the planar S_2 ($1^1\pi\pi^*$) state, in which the π and π^* orbitals are delocalised over the entire molecule. PCET is mediated by coupling and subsequent IC to a (optically dark) $S_1(1^1n\pi^*)$ state, which develops progressive charge transfer character upon migration of the proton from the OH to the CO, on a ~100 fs timescale. The S_1 state links to the S_0 state *via* a $1^1n\pi^*/S_0$ CI, the minimum energy geometry of which requires loss of planarity (one ring twists relative to the other about the central aliphatic C–C bond). Following IC, the time constant for which is ~400 fs, reverse H atom transfer on the S_0 PES and vibrational energy transfer to the surrounding solvent results in reformation of the original enol isomer with a (solvent dependent) time constant in the range ~5–8 ps. The ground state population does not fully recover within the maximum available experimental time delay (2 ns), leading to the suggestion that ~10% of the excited state molecules form a photoproduct. Transient vibrational absorption studies identify the presence of the *E*-keto isomer (a logical product following full 180° rotation about the C–C bond).[110,204] Other studies have suggested some phenoxyl radical formation.[205] DOB and SB are structurally similar to OB, and we thus anticipate similarities in the decay mechanisms of their excited states formed upon exposure to UV-A/-B.[205]

Our final case study is avobenzone (AB). AB also has obvious structural similarities with OB but, as Fig. 14 shows, its lowest energy tautomer lacks an OH group. Nonetheless, AB tends to exist in a H-bonded enol form (characterised by an intramolecular H-bond),[206] and the most detailed current picture regarding its excited state photophysics stems from transient absorption studies of AB in cyclohexane, acetonitrile and methanol by Crim and coworkers.[207] The excited H-bonded enol form (termed a chelated enol in the original work)[207] of AB formed by absorption of a 350 nm photon is deduced to decay on a sub-ps timescale, yielding several different non-H-bonded (or non-chelated) enols. One of the proposed non-H bonded structures simply involves 180° torsion of the O–H bond, but others involve $E \rightarrow Z$ isomerism about the C–C bond adjacent to one or other carbonyl group. The relative yields of these various non-H-bonded forms, and the rates with which they relax to the starting S_0 (H-bonded) state are sensitive to the choice of solvent.[206,207] As in so many of these examples, complete ground state recovery is not observed, implying some (low) probability for forming a long-lived photoproduct, possibly a stable keto-AB isomer.[207,208]

5. Discussion

Manipulating the photostability and efficacy of chemical filters

One key consideration in any sunscreen development is that a filter should absorb at the relevant UV-A/-B wavelengths, be photostable, and exhibit one or more efficient, non-radiative, photodeactivation pathways.[48] The examples considered in this review display such pathways, but identifying and understanding what characteristics are key to ensuring the required photostability and photoprotective efficiency in one chemical filter could guide our manipulation of such properties in another. As shown in Section 4, details of the excited state photophysics can vary with choice of solvent and/or the solvent polarity,[207,209] but this is unlikely to be a viable option for a commercial product.

Another manipulation strategy could be to alter the electron density distribution in the filter molecule by, for example, chemical substitution. Simply introducing an electron donating

or withdrawing group – at ring positions remote from the reaction coordinate – has been shown to have major impact on the rate of the $\pi\sigma^*$ state-mediated O–H bond fission process in a range of substituted phenols.[210] It is not unrealistic to imagine that a similar aromatic substitution strategy might affect the UV photodynamics displayed by, for example, some of the cinnamate species used as chemical filters – boosting their deactivation efficiency by, for example, increasing the relaxation rate and/or the probability of parent ground state recovery.

Pursuing a synthetic line of thinking further, can we learn from nature and improve the photostability of a given chemical filter by coupling the monomer units – covalently, as in DHICA,[182,211] or non-covalently,[212] as in the case of the DNA-bases? Such questions apply not just to chemical filters currently used in sunscreen formulations but also, and perhaps more importantly, to potential filters that might have been investigated in the past and rejected on the basis that they displayed inadequate photostability when in monomer form.

Outlook of challenges and future prospects

This review began by summarising the natural photoprotective mechanisms shown by humans in response to changing levels of UVR, and highlighted situations when such mechanisms are inadequate and the burden-of-disease increases (Fig. 1). Sunscreens are now the almost universal solution to pre-empting overexposure to UVR. Given their prevalence, it is perhaps inevitable that the efficacy and the health consequences of sunscreen use continue to attract close scrutiny.[12,14,15]

This review focuses on the photophysical properties of chemical filters, and how these are increasingly being revealed using combinations of theory and ultrafast laser chemistry. Gas-phase measurements together with *ab initio* electronic structure calculations can reveal the ultrafast excited state photophysics in isolated chemical filter molecules. Solution-phase studies take us a step closer to the actual environment in which such chemical filters are used as a sunscreen, and allow study of the full deactivation pathway back to the starting ground state molecule. Such studies provide a useful first cut at assessing the likely efficacy of a chemical filter, and to screen for the formation of rival photoproducts – which can be the root cause of some of the adverse effects associated with sunscreen use.[54]

Following such a 'bottom-up' approach has resulted in impressive advances in our understanding of the ultrafast decay following UV photoexcitation of many of these chemical filters, but many questions remain to be answered before we can start to claim to understand the full gamut of photoprotective mechanisms provided in nature. This review ends by outlining some of the outstanding questions.

(i) Given that sunscreen products contain many tens of individual components, how are the dynamics of one component affected by the presence of another? This question is not new. Many components are included in commercial sunscreens in particular combinations precisely because of the way they interact. Adding octocrylene, for example, is a recognised route to enhancing the photostability of avobenzone.[48,213–216] The interactions between different ingredients need not be synergistic, however, so it remains important to examine the behaviour of one component in the presence of others. Extending the types of experimental study reviewed here to include multiple components is relatively simple if the signals from each are well separated – spectrally or temporally – as demonstrated, for example, by our own recent ultrafast UV pump–probe studies of oxybenzone in the presence of titanium dioxide (one of the commonly used inorganic filters).[217]

(ii) Are any photoproducts safe? Many studies deduce (*via* observation of an incomplete ground state bleach recovery) or actually observe photoproduct formation. Identifying that photoproduct can be challenging, however. NMR and GC-MS have shown success in identifying products after photoexcitation.[123,218] Identification alone does not ensure adequate evaluation of the safety of the component in a sunscreen product, however. Any full assessment also requires that we investigate the fates of the (potentially reactive) excited states formed when these photoproducts themselves interact with UV light. This could be problematic if photoexcitation results in radical formation, for example. Armed with such knowledge, however, it may be possible to mitigate the problem by adding a suitable radical scavenger species to the blend. Further, we recognise that natural sunscreens such as melanins are continually replaced as they degrade. Conventional sunscreen products, in contrast, require frequent re-applications. A robust sunscreen that requires less frequent replacement would be particularly attractive to the end-user.

(iii) If, as has been demonstrated in several cases within this review, the excited state dynamics displayed by a chemical filter change upon switching from the gas- to solution-phase, what happens in an actual sunscreen product? Unarguably, studying the chemical filter in the solution-phase provides a better approximation (*cf.* the gas-phase) of the environment prevailing in a sunscreen, but it is still quite far from the case of the chemical filter in a formulation containing many other components in the form of an oil or paste. The challenge presented by multi-molecular systems has been touched on in (i) above, but the fact that the solution-phase remains a poor mimic of the native environment in a commercial product still needs to be addressed. Studies involving thin-film samples are a logical next step,[157,219] while clinical trials involving skin samples will inevitably remain necessary for evaluating the safety and efficacy of any product in ways that are not assessable *via* any of the photophysical techniques considered in this review.

Acknowledgements

We are grateful to the Engineering and Physical Sciences Research Council for the following funding: EP/L005913 (Bristol), EP/J007153 (Warwick) and EP/F500378 (that provides a studentship for L. A. B.). V. G. S. is grateful to the Royal Society and the Leverhulme Trust for a Royal Society Leverhulme Trust Senior Research Fellowship, and B. M. and T. N. V. K. are both grateful to the Technical University of Munich for awards of T. U. Munich Fellowships.

Notes and references

1 A. S. Aldahan, V. V. Shah, S. Mlacker and K. Nouri, *JAMA Dermatol.*, 2015, **151**, 1316.
2 C. D. Kaur and S. Saraf, *Pharmacogn. Res.*, 2010, **2**, 22–25.
3 A. Maciejewski, R. Naskrecki, M. Lorenc, M. Ziolek, J. Karolczak, J. Kubicki, M. Matysiak and M. Szymanski, *J. Mol. Struct.*, 2000, **555**, 1–13.
4 F. Urbach, *J. Photochem. Photobiol., B*, 2001, **64**, 99–104.
5 P. E. Hockberger, *Photochem. Photobiol.*, 2002, **76**, 561–579.
6 M. Lorenzen, V. Racicot, D. Strack and C. Chapple, *Plant Physiol.*, 1996, **112**, 1625–1630.
7 A. Bachem and B. Fantus, *Arch. Phys. Ther.*, 1939, **20**, 69–76.
8 U. Henschke, *Strahlentherapie*, 1940, **67**, 659–667.
9 A. C. Giese, E. Christensen and J. Jeppard, *J. Am. Pharm. Assoc.*, 1950, **39**, 30–36.
10 N. J. Lowe, *Dermatol. Clin.*, 2006, **24**, 9–17.
11 J. M. Knox, A. C. Griffin and R. E. Hakim, *J. Invest. Dermatol.*, 1960, **34**, 51–58.
12 M. Lodèn, H. Beitner, H. Gonzalez, D. W. Edström, U. Åkerström, J. Austad, I. Buraczewska-Norin, M. Matsson and H. C. Wulf, *Br. J. Dermatol.*, 2011, **165**, 255–262.
13 R. Jansen, U. Osterwalder, S. Q. Wang, M. Burnett and H. W. Lim, *J. Am. Acad. Dermatol.*, 2013, **69**, 867.
14 S. E. Mancebo, J. Y. Hu and S. Q. Wang, *Dermatol. Clin.*, 2014, **32**, 427–438.
15 M. E. Burnett and S. Q. Wang, *Photodermatol., Photoimmunol. Photomed.*, 2011, **27**, 58–67.
16 M. Linh Tran, B. J. Powell and P. Meredith, *Biophys. J.*, 2006, **90**, 743–752.
17 L. A. Baker, M. D. Horbury, S. E. Greenough, F. Allais, P. S. Walsh, S. Habershon and V. G. Stavros, *J. Phys. Chem. Lett.*, 2016, **7**, 56–61.
18 J. F. Kasting and J. L. Siefert, *Science*, 2002, **296**, 1066–1068.
19 R. P. Sinha and D.-P. Häder, *Photochem. Photobiol. Sci.*, 2002, **1**, 225–236.
20 A. Sancar, L. A. Lindsey-Boltz, K. Ünsal-Kaçmaz and S. Linn, *Annu. Rev. Biochem.*, 2004, **73**, 39–85.
21 R. Lucas, T. McMichael, W. Smith and B. Armstrong, *Solar Ultraviolet Radiation. Global burden of disease from solar ultraviolet radiation*, World Health Organization, Geneva, 2006.
22 M. F. Holick, *Am. J. Clin. Nutr.*, 2004, **80**, 1678S–1688S.
23 M. F. Holick, *N. Engl. J. Med.*, 2007, **357**, 266–281.
24 L. A. Baker and V. G. Stavros, *Sci. Prog.*, 2016, **99**, 282–311.
25 R. S. Mason and J. Reichrath, *Adv. Anticancer Agents Med. Chem.*, 2013, **13**, 83–97.
26 A. Slominski, D. J. Tobin, S. Shibahara and J. Wortsman, *Physiol. Rev.*, 2004, **84**, 1155–1228.
27 H. Fedorow, F. Tribl, G. Halliday, M. Gerlach, P. Riederer and K. L. Double, *Prog. Neurobiol.*, 2005, **75**, 109–124.
28 S. Ito, *Pigm. Cell Res.*, 2003, **16**, 230–236.
29 K. Wakamatsu and S. Ito, *Pigm. Cell Res.*, 2002, **15**, 174–183.
30 M. Cichorek, M. Wachulska, A. Stasiewicz and A. Tymińska, *Postępy. Dermatol. Alergol.*, 2013, **30**, 30–41.
31 M. Brenner and V. J. Hearing, *Photochem. Photobiol.*, 2008, **84**, 539–549.
32 X. Wu and J. A. Hammer, *Curr. Opin. Cell Biol.*, 2014, **29**, 1–7.
33 H. Ando, Y. Niki, M. Yoshida, M. Ito, K. Akiyama, J.-H. Kim, T.-J. Yoon, M. S. Matsui, D. B. Yarosh and M. Ichihashi, *Cell. Logist.*, 2011, **1**, 12–20.
34 J. P. Ortonne, *Br. J. Dermatol.*, 2002, **146**, 7–10.
35 H. Y. Park, M. Kosmadaki, M. Yaar and B. A. Gilchrest, *Cell. Mol. Life Sci.*, 2009, **66**, 1493–1506.
36 S. Premi, S. Wallisch, C. M. Mano, A. B. Weiner, A. Bacchiocchi, K. Wakamatsu, E. J. H. Bechara, R. Halaban, T. Douki and D. E. Brash, *Science*, 2015, **347**, 842–847.
37 U. Osterwalder, M. Sohn and B. Herzog, *Photodermatol., Photoimmunol. Photomed.*, 2014, **30**, 62–80.
38 G. I. Jenkins, *Annu. Rev. Plant Biol.*, 2009, **60**, 407–431.
39 H. Frohnmeyer and D. Staiger, *Plant Physiol.*, 2003, **133**, 1420–1428.
40 K. Meyer, J. C. Cusumano, C. Somerville and C. C. S. Chapple, *Proc. Natl. Acad. Sci. U. S. A.*, 1996, **93**, 6869–6874.
41 C. M. Fraser and C. Chapple, *Arabidopsis Book*, 2011, vol. 9, p. e0152.
42 M. S. Eller and B. A. Gilchrest, *Pigm. Cell Res.*, 2000, **13**, 94–97.
43 J. A. Levine, M. Sorace, J. Spencer and D. M. Siegel, *J. Am. Acad. Dermatol.*, 2005, **53**, 1038–1044.
44 N. A. Kasparian, J. K. McLoone and B. Meiser, *J. Behav. Med.*, 2009, **32**, 406–428.
45 M. D. Palm and M. N. O'Donoghue, *Dermatol. Ther.*, 2007, **20**, 360–376.
46 S. González, M. Fernández-Lorente and Y. Gilaberte-Calzada, *Clin. Dermatol.*, 2008, **26**, 614–626.
47 S. Q. Wang, Y. Balagula and U. Osterwalder, *Dermatol. Ther.*, 2010, **23**, 31–47.
48 S. Forestier, *J. Am. Acad. Dermatol.*, 2008, **58**, S133–S138.
49 J. S. Adams and M. Hewison, *J. Clin. Endocrinol. Metab.*, 2010, **95**, 471–478.
50 M. I. Cabrera, O. M. Alfano and A. E. Cassano, *J. Phys. Chem.*, 1996, **100**, 20043–20050.
51 R. L. Siegel, K. D. Miller and A. Jemal, *Ca-Cancer J. Clin.*, 2016, **66**, 7–30.
52 T. G. Smijs and S. Pavel, *Nanotechnol., Sci. Appl.*, 2011, **4**, 95–112.
53 M. Krause, A. Klit, M. B. Jensen, T. Søeborg, H. Frederiksen, M. Schlumpf, W. Lichtensteiger, N. E. Skakkebaek and K. T. Drzewiecki, *Int. J. Androl.*, 2012, **35**, 424–436.
54 J. F. Nash and P. R. Tanner, *Photoder*, 2014, **30**, 88–95.
55 A. Jabloński, *Nature*, 1933, **131**, 839–840.
56 N. J. Turro, V. Ramamurthy and J. C. Scaiano, *Principles of Molecular Photochemistry: An Introduction*, University Science Books, 2009.
57 F. Bernardi, M. Olivucci and M. A. Robb, *Chem. Soc. Rev.*, 1996, **25**, 321–328.
58 G. A. Worth and L. S. Cederbaum, *Annu. Rev. Phys. Chem.*, 2004, **55**, 127–158.
59 S. Matsika and P. Krause, *Annu. Rev. Phys. Chem.*, 2011, **62**, 621–643.
60 D. R. Yarkony, *Rev. Mod. Phys.*, 1996, **68**, 985–1013.

61 S. E. Greenough, M. D. Horbury, J. O. F. Thompson, G. M. Roberts, T. N. V. Karsili, B. Marchetti, D. Townsend and V. G. Stavros, *Phys. Chem. Chem. Phys.*, 2014, **16**, 16187–16195.
62 D. Murdock, S. J. Harris, T. N. V. Karsili, G. M. Greetham, I. P. Clark, M. Towrie, A. J. Orr-Ewing and M. N. R. Ashfold, *J. Phys. Chem. Lett.*, 2012, **3**, 3715–3720.
63 R. Schinke, *Photodissociation Dynamics*, Cambridge University Press, Cambridge, 1993.
64 V. Engel, V. Staemmler, R. L. Vanderwal, F. F. Crim, R. J. Sension, B. Hudson, P. Andresen, S. Hennig, K. Weide and R. Schinke, *J. Phys. Chem.*, 1992, **96**, 3201–3213.
65 M. N. R. Ashfold, D. H. Mordaunt and S. H. S. Wilson, *Advances in Photochemistry*, John Wiley and Sons, New York, 1996.
66 M. N. R. Ashfold and S. R. Langford, *The Role of Rydberg States in Spectroscopy and Photochemistry*, Kluwer Academic Press, Dordrecht, Netherlands, 1999.
67 S. A. Harich, D. W. H. Hwang, X. F. Yang, J. J. Lin, X. M. Yang and R. N. Dixon, *J. Chem. Phys.*, 2000, **113**, 10073–10090.
68 S. Satyapal, J. Park, R. Bersohn and B. Katz, *J. Chem. Phys.*, 1989, **91**, 6873–6879.
69 Y. Wen, J. Segall, M. Dulligan and C. Wittig, *J. Chem. Phys.*, 1994, **101**, 5665–5671.
70 S.-H. Lee, H.-I. Lee and Y. T. Lee, *J. Chem. Phys.*, 2004, **121**, 11053–11059.
71 S. Harich, J. J. Lin, Y. T. Lee and X. Yang, *J. Phys. Chem. A*, 1999, **103**, 10324–10332.
72 K. J. Yuan, Y. Cheng, F. Y. Wang and X. M. Yang, *Chin. J. Chem. Phys.*, 2008, **21**, 301–307.
73 S. H. S. Wilson, J. D. Howe and M. N. R. Ashfold, *Mol. Phys.*, 1996, **88**, 841–848.
74 M. N. R. Ashfold, G. A. King, D. Murdock, M. G. D. Nix, T. A. A. Oliver and A. G. Sage, *Phys. Chem. Chem. Phys.*, 2010, **12**, 1218–1238.
75 C. Xie, J. Ma, X. Zhu, D. R. Yarkony, D. Xie and H. Guo, *J. Am. Chem. Soc.*, 2016, **138**, 7828–7831.
76 X. Xu, J. Zheng, K. R. Yang and D. G. Truhlar, *J. Am. Chem. Soc.*, 2014, **136**, 16378–16386.
77 G. M. Roberts, A. S. Chatterley, J. D. Young and V. G. Stavros, *J. Phys. Chem. Lett.*, 2012, **3**, 348–352.
78 C. Ratzer, J. Kupper, D. Spangenberg and M. Schmitt, *Chem. Phys.*, 2002, **283**, 153–169.
79 M. G. D. Nix, A. L. Devine, B. Cronin, R. N. Dixon and M. N. R. Ashfold, *J. Chem. Phys.*, 2006, **125**, 133318.
80 R. N. Dixon, T. A. A. Oliver and M. N. R. Ashfold, *J. Chem. Phys.*, 2011, **134**, 194303.
81 Y. Zhang, T. A. A. Oliver, M. N. R. Ashfold and S. E. Bradforth, *Faraday Discuss.*, 2012, **157**, 141–163.
82 S. Perun, A. L. Sobolewski and W. Domcke, *J. Am. Chem. Soc.*, 2005, **127**, 6257–6265.
83 S. Yamazaki, W. Domcke and A. L. Sobolewski, *J. Phys. Chem. A*, 2008, **112**, 11965–11968.
84 V. B. Delchev, A. L. Sobolewski and W. Domcke, *Phys. Chem. Chem. Phys.*, 2010, **12**, 5007–5015.
85 B. Marchetti, T. N. V. Karsili, M. N. R. Ashfold and W. Domcke, *Phys. Chem. Chem. Phys.*, 2016, **18**, 20007–20027.
86 R. J. Harrison, G. I. Fann, T. Yanai and Z. Gan, *J. Chem. Phys.*, 2004, **121**, 11587–11598.
87 S. Gozem, F. Melaccio, H. L. Luk, S. Rinaldi and M. Olivucci, *Chem. Soc. Rev.*, 2014, **43**, 4019–4036.
88 A. L. Sobolewski and W. Domcke, *Phys. Chem. Chem. Phys.*, 2004, **6**, 2763–2771.
89 A. L. Sobolewski and W. Domcke, *Chem. Phys. Lett.*, 1993, **211**, 82–87.
90 A. L. Sobolewski, *Chem. Phys. Lett.*, 1993, **211**, 293–299.
91 A. L. Sobolewski and W. Domcke, *Chem. Phys.*, 1994, **184**, 115–124.
92 Z. Lan, L. M. Frutos, A. L. Sobolewski and W. Domcke, *Proc. Natl. Acad. Sci. U. S. A.*, 2008, **105**, 12707–12712.
93 S. Perun and A. L. Sobolewski, *J. Phys. Chem. A*, 2006, **110**, 9031–9038.
94 A. L. Sobolewski, W. Domcke and C. Hättig, *Proc. Natl. Acad. Sci. U. S. A.*, 2005, **102**, 17903–17906.
95 N. das Neves Rodriguez, M. Staniforth and V. G. Stavros, *Proc. R. Soc. A*, 2016, **472**, 0677.
96 E. G. Buchanan, W. H. James III, S. H. Choi, L. Guo, S. H. Gellman and C. W. Müller, *J. Chem. Phys.*, 2012, **137**, 094301.
97 C.-M. Tseng, Y. T. Lee, M.-F. Lin, C.-K. Ni, S.-Y. Liu, Y.-P. Lee, Z. F. Xu and M. C. Lin, *J. Phys. Chem. A*, 2007, **111**, 9463–9470.
98 T. S. Zwier, *J. Phys. Chem. A*, 2006, **110**, 4133–4150.
99 X. M. Yang, *Int. Rev. Phys. Chem.*, 2005, **24**, 37–98.
100 J. Wei, A. Kuczmann, J. Riedel, F. Renth and F. Temps, *Phys. Chem. Chem. Phys.*, 2003, **5**, 315–320.
101 D. A. Blank, S. W. North and Y. T. Lee, *Chem. Phys.*, 1994, **187**, 35–47.
102 H. Lippert, H.-H. Ritze, I. V. Hertel and W. Radloff, *ChemPhysChem*, 2004, **5**, 1423–1427.
103 R. Montero, Á. P. Conde, V. Ovejas, M. Fernández-Fernández, F. Castaño, J. R. Vázquez de Aldana and A. Longarte, *J. Chem. Phys.*, 2012, **137**, 064317.
104 A. Maciejewski, R. Naskrecki, M. Lorenc, M. Ziolek, J. Karolczak, J. Kubicki, M. Matysiak and M. Szymanski, *J. Mol. Struct.*, 2000, **555**, 1–13.
105 R. Berera, R. van Grondelle and J. T. M. Kennis, *Photosynth. Res.*, 2009, **101**, 105–118.
106 U. Megerle, I. Pugliesi, C. Schriever, C. Sailer and E. Riedle, *Appl. Phys. B: Lasers Opt.*, 2003, **96**, 215–231.
107 M. Towrie, D. C. Grills, J. Dyer, J. A. Weinstein, P. Matousek, R. Barton, P. D. Bailey, N. Subramaniam, W. M. Kwok, C. Ma, D. Phillips, A. W. Parker and M. W. George, *Appl. Spectrosc.*, 2003, **57**, 367–380.
108 G. M. Roberts, H. J. B. Marroux, M. P. Grubb, M. N. R. Ashfold and A. J. Orr-Ewing, *J. Phys. Chem. A*, 2014, **118**, 11211–11225.
109 Y. Zhang, K. de La Harpe, A. A. Beckstead, R. Improta and B. Kohler, *J. Am. Chem. Soc.*, 2015, **137**, 7059–7062.
110 L. A. Baker, M. D. Horbury, S. E. Greenough, P. M. Coulter, T. N. V. Karsili, G. M. Roberts, A. J. Orr-Ewing, M. N. R. Ashfold and V. G. Stavros, *J. Phys. Chem. Lett.*, 2015, **6**, 1363–1368.

111 A. S. Chatterley, C. W. West, V. G. Stavros and J. R. R. Verlet, *Chem. Sci.*, 2014, **5**, 3963–3975.
112 S. C. Warren, A. Margineanu, D. Alibhai, D. J. Kelly, C. Talbot, Y. Alexandrov, I. Munro, M. Katan, C. Dunsby and P. M. W. French, *PLoS One*, 2013, **8**, e70687.
113 T. A. Roelofs, C.-H. Lee and A. R. Holzwarth, *Biophys. J.*, 1992, **61**, 1147–1163.
114 J. J. Snellenburg, S. Laptenok, R. Seger, K. M. Mullen and I. H. M. Van Stokkum, *J. Stat. Softw.*, 2012, **49**, 1–22.
115 G. M. Roberts and V. G. Stavros, *Chem. Sci.*, 2014, **5**, 1698–1722.
116 V. G. Stavros and J. R. R. Verlet, *Annu. Rev. Phys. Chem.*, 2016, **67**, 211–232.
117 B. Schmidt, S. Laimgruber, W. Zinth and P. A. Gilch, *Appl. Phys. B: Lasers Opt.*, 2003, **76**, 809–814.
118 M. Sajadi, A. Dobryakov, E. Garbin, N. Ernsting and S. Kovalenko, *Chem. Phys. Lett.*, 2010, **489**, 44–47.
119 A. Cannizzo, O. Bräm, G. Zgrablic, A. Tortschanoff, A. A. Oskouei, F. van Mourik and M. Chergui, *Opt. Lett.*, 2007, **32**, 3555–3557.
120 M. Gerecke, G. Bierhance, M. Gutmann, N. P. Ernsting and A. Rosspeintner, *Rev. Sci. Instrum.*, 2016, **87**, 053115.
121 P. Kukura, D. W. McCamant and R. A. Mathies, *Annu. Rev. Phys. Chem.*, 2007, **58**, 461–488.
122 K. M. Hanson, S. Narayanan, V. M. Nichols and C. J. Bardeen, *Photochem. Photobiol. Sci.*, 2015, **14**, 1607–1616.
123 Y. Peperstraete, M. Staniforth, L. A. Baker, N. D. N. Rodrigues, N. C. Cole-Filipiak, W.-D. Quan and V. G. Stavros, *Phys. Chem. Chem. Phys.*, 2016, **18**, 28140–28149.
124 B. O. Roos, P. R. Taylor and P. E. M. Siegbahn, *Chem. Phys.*, 1980, **48**, 157–173.
125 L. M. Cheung, K. R. Sundberg and K. Ruedenberg, *J. Am. Chem. Soc.*, 1978, **100**, 8024–8025.
126 J. Finley, P.-Å. Malmqvist, B. O. Roos and L. Serrano-Andrés, *Chem. Phys. Lett.*, 1998, **288**, 299–306.
127 K. Andersson and B. O. Roos, Multiconfigurational second-order perturbation theory, *Modern Electronic Structure Theory*, World Scientific, 1995.
128 K. Ruedenberg, M. W. Schmidt, M. M. Gilbert and S. T. Elbert, *Chem. Phys.*, 1982, **71**, 41–49.
129 P. Hohenberg and W. Kohn, *Phys. Rev.*, 1964, **136**, B864–B871.
130 E. Runge and E. K. U. Gross, *Phys. Rev. Lett.*, 1984, **52**, 997–1000.
131 J. F. Stanton and R. J. Bartlett, *J. Chem. Phys.*, 1993, **98**, 7029–7039.
132 P. Baudin, J. Sánchez Marín, I. García Cuesta and A. M. Sánchez de Merás, *J. Chem. Phys.*, 2014, **140**, 104111.
133 A. Dreuw and M. Wormit, *Wiley Interdiscip. Rev.: Comput. Mol. Sci.*, 2015, **5**, 82–95.
134 D. Tuna, N. Došlić, M. Mališ, A. L. Sobolewski and W. Domcke, *J. Phys. Chem. B*, 2015, **119**, 2112–2124.
135 D. Tuna, A. L. Sobolewski and W. Domcke, *J. Phys. Chem. A*, 2014, **118**, 122–127.
136 S. Chaiwongwattana, M. Sapunar, A. Ponzi, P. Decleva and N. Došlić, *J. Phys. Chem. A*, 2015, **119**, 10637–10644.
137 M. Barbatti, *J. Am. Chem. Soc.*, 2014, **136**, 10246–10249.
138 B. R. Brooks, R. E. Bruccoleri, B. D. Olafson, D. J. States, S. Swaminathan and M. Karplus, *J. Comput. Chem.*, 1983, **4**, 187–217.
139 P. Ren and J. W. Ponder, *J. Phys. Chem. B*, 2003, **107**, 5933–5947.
140 J. C. Phillips, R. Braun, W. Wang, J. Gumbart, E. Tajkhorshid, E. Villa, C. Chipot, R. D. Skeel and L. Kalé, *J. Comput. Chem.*, 2005, **26**, 1781–1802.
141 S. Metz, J. Kästner, A. A. Sokol, T. W. Keal and P. Sherwood, *Wiley Interdiscip. Rev.: Comput. Mol. Sci.*, 2014, **4**, 101–110.
142 J. N. Harvey, *Faraday Discuss.*, 2004, **127**, 165–177.
143 J. C. Tully, *J. Chem. Phys.*, 1990, **93**, 1061–1071.
144 M. Barbatti, M. Ruckenbauer, F. Plasser, J. Pittner, G. Granucci, M. Persico and H. Lischka, *Wiley Interdiscip. Rev.: Comput. Mol. Sci.*, 2014, **4**, 26–33.
145 L. Du and Z. Lan, *J. Chem. Theory Comput.*, 2015, **11**, 1360–1374.
146 M. Richter, P. Marquetand, J. González-Vázquez, I. Sola and L. González, *J. Chem. Theory Comput.*, 2011, **7**, 1253–1258.
147 J. W. Snyder, B. F. E. Curchod and T. J. Martínez, *J. Phys. Chem. Lett.*, 2016, **7**, 2444–2449.
148 E. G. Hohenstein, *J. Am. Chem. Soc.*, 2016, **138**, 1868–1876.
149 W. Boerjan, J. Ralph and M. Baucher, *Annu. Rev. Plant Biol.*, 2003, **54**, 519–546.
150 D. V. Evtuguin and F. M. L. Amado, *Macromol. Biosci.*, 2003, **7**, 339–343.
151 J. D. Gargulak, S. E. Lebo and T. J. McNally, *Lignin*, Kirk-Othmer Encyclopedia of Chemical Technology, 2015.
152 C. P. Rodrigo, W. H. James and T. S. Zwier, *J. Am. Chem. Soc.*, 2011, **133**, 2632–2641.
153 J. D. Young, M. Staniforth, J. C. Dean, G. M. Roberts, F. Mazzoni, T. N. V. Karsili, M. N. R. Ashfold, T. S. Zwier and V. G. Stavros, *J. Phys. Chem. Lett.*, 2014, **5**, 2138–2143.
154 B. George, E. Suttie, A. Merlin and X. Deglise, *Polym. Degrad. Stab.*, 2005, **2**, 268–274.
155 M. Baucher, B. Monties, M. V. Montagu and W. Boerjan, *Crit. Rev. Plant Sci.*, 1998, **2**, 125–197.
156 Y. Zhang, T. A. A. Oliver, M. N. R. Ashfold and S. E. Bradforth, *Faraday Discuss.*, 2012, **157**, 141–163.
157 L. A. Baker, S. E. Greenough and V. G. Stavros, *J. Phys. Chem. Lett.*, 2016, **7**, 4655–4665.
158 J. C. Dean, R. Kusaka, P. S. Walsh, F. Allais and T. S. Zwier, *J. Am. Chem. Soc.*, 2014, **136**, 14780–14795.
159 F. Liu, L. Du, Z. Lan and J. Gao, *Photochem. Photobiol. Sci.*, 2017, **16**, 211–219.
160 T. Gustavsson, R. Improta and D. Markovitsi, *J. Phys. Chem. Lett.*, 2010, **1**, 2025–2030.
161 R. Improta, F. Santoro and L. Blancafort, *Chem. Rev.*, 2016, **116**, 3540–3593.
162 B. Kohler, *J. Phys. Chem. Lett.*, 2010, **1**, 2047–2053.
163 C. E. Crespo-Hernández, B. Cohen, P. M. Hare and B. Kohler, *Chem. Rev.*, 2004, **104**, 1977–2020.
164 K. Röttger, H. J. B. Marroux, M. P. Grubb, P. M. Coulter, H. Böhnke, A. S. Henderson, M. C. Galan, F. Temps,

A. J. Orr-Ewing and G. M. Roberts, *Angew. Chem., Int. Ed.*, 2015, **54**, 14719–14722.
165 R. W. Schoenlein, L. A. Peteanu, R. A. Mathies and C. V. Shank, *Science*, 1991, **254**, 412–415.
166 T. Kobayashi, T. Saito and H. Ohtani, *Nature*, 2001, **414**, 531–534.
167 N. Ferré and M. Olivucci, *J. Am. Chem. Soc.*, 2003, **125**, 6868–6869.
168 D. Polli, P. Altoè, O. Weingart, K. M. Spillane, C. Manzoni, D. Brida, G. Tomasello, G. Orlandi, P. Kukura, R. A. Mathies, M. Garavelli and G. Cerullo, *Nature*, 2010, **467**, 440–443.
169 I. Schapiro, M. N. Ryazantsev, L. M. Frutos, N. Ferré, R. Lindh and M. Olivucc, *J. Am. Chem. Soc.*, 2011, **133**, 3354–3364.
170 S. Gozem, F. Melaccio, R. Lindh, A. I. Krylov, A. A. Granovsky, C. Angeli and M. Olivucci, *J. Chem. Theory Comput.*, 2013, **9**, 4495–4506.
171 G. Bassolino, T. Sovdat, A. S. Duarte, J. M. Lim, C. Schnedermann, M. Liebel, B. Odell, T. D. W. Claridge, S. P. Fletcher and P. Kukura, *J. Am. Chem. Soc.*, 2015, **137**, 12434–12437.
172 P. S. Sherin, J. Grilj, Y. P. Tsentalovich and E. Vauthey, *J. Phys. Chem. B*, 2009, **113**, 4953–4962.
173 D. Tuna, A. L. Sobolewski and W. Domcke, *J. Phys. Chem. B*, 2014, **118**, 976–985.
174 L. Zhao, P.-W. Zhou and G.-J. Zhao, *J. Chem. Phys.*, 2016, **145**, 044316.
175 B. Marchetti and T. N. V. Karsili, *Phys. Chem. Chem. Phys.*, 2016, **18**, 3644–3658.
176 J. Peon, G. C. Hess, J.-M. L. Pecourt, T. Yuzawa and B. Kohler, *J. Phys. Chem. A*, 1999, **103**, 2460–2466.
177 M. Gauden, A. Pezzella, L. Panzella, A. Napolitano, M. d'Ischia and V. Sundström, *J. Phys. Chem. B*, 2009, **113**, 12575–12580.
178 A. Huijser, A. Pezzella, J. K. Hannestad, L. Panzella, A. Napolitano, M. d'Ischia and V. Sundström, *ChemPhysChem*, 2010, **11**, 2424–2431.
179 A. Corani, A. Pezzella, T. Pascher, T. Gustavsson, D. Markovitsi, A. Huijser, M. d'Ischia and V. Sundström, *J. Phys. Chem. Lett.*, 2013, **4**, 1383–1388.
180 A. L. Sobolewski and W. Domcke, *ChemPhysChem*, 2007, **8**, 756–762.
181 A. Huijser, A. Pezzellab and V. Sundström, *Phys. Chem. Chem. Phys.*, 2011, **13**, 9119–9127.
182 A. Corani, A. Huijser, T. Gustavsson, D. Markovitsi, P.-Å. Malmqvist, A. Pezzella, M. d'Ischia and V. Sundström, *J. Am. Chem. Soc.*, 2014, **136**, 11626–11635.
183 V. E. Reeve, G. E. Greenoak, P. J. Canfield, C. Boehm-Wilcox and C. H. Gallagher, *Photochem. Photobiol.*, 1989, **49**, 459–464.
184 S. Beissert and K. Loser, *Photochem. Photobiol.*, 2008, **84**, 29–34.
185 D. Tuna, A. Udvarhelyi, A. L. Sobolewski, W. Domcke and T. Domratcheva, *J. Phys. Chem. B*, 2016, **120**, 3493–3502.
186 C. Anselmi, M. Centini, M. Maggiore, N. Gaggelli, M. Andreassi, A. Buonocore, G. Beretta and R. M. Facino, *J. Pharm. Biomed. Anal.*, 2008, **46**, 645–652.
187 G. A. King, T. A. A. Oliver, R. N. Dixon and M. N. R. Ashfold, *Phys. Chem. Chem. Phys.*, 2012, **14**, 3338–3345.
188 A. S. Chatterley, J. D. Young, D. Townsend, J. M. Żurek, M. J. Paterson, G. M. Roberts and V. G. Stavros, *Phys. Chem. Chem. Phys.*, 2013, **15**, 6879–6892.
189 D. J. Hadden, C. A. Williams, G. M. Roberts and V. G. Stavros, *Phys. Chem. Chem. Phys.*, 2011, **13**, 4494–4499.
190 G. Prampolini, I. Cacelli and A. Ferretti, *RSC Adv.*, 2015, **5**, 38513–38526.
191 T. N. V. Karsili, B. Marchetti, M. N. R. Ashfold and W. Domcke, *J. Phys. Chem. A*, 2014, **118**, 11999–12010.
192 G. Mazzone, N. Russo and M. Toscano, *Comput. Theor. Chem.*, 2016, **1077**, 39–47.
193 A. Urbaniak, M. Szeląg and M. Molski, *Comput. Theor. Chem.*, 2013, **1012**, 33–40.
194 E. M. M. Tan, M. Hilbers and W. J. Buma, *J. Phys. Chem. Lett.*, 2014, **5**, 2464–2468.
195 E. V. Gromov, I. Burghardt, J. T. Hynes, H. Köppel and L. S. Cederbaum, *J. Photochem. Photobiol., A*, 2007, **190**, 241–257.
196 X.-P. Chang, C.-X. Li, B.-B. Xie and G. Cui, *J. Phys. Chem. A*, 2015, **119**, 11488–11497.
197 E. M. M. Tan, S. Amirjalayer, B. H. Bakker and W. J. Buma, *Faraday Discuss.*, 2013, **163**, 321–340.
198 Y. Miyazaki, K. Yamamoto, J. Aoki, T. Ikeda, Y. Inokuchi, M. Ehara and T. Ebata, *J. Chem. Phys.*, 2014, **141**, 244313.
199 K. Yamazaki, Y. Miyazaki, Y. Harabuchi, T. Taketsugu, S. Maeda, Y. Inokuchi, S. Kinoshita, M. Sumida, Y. Onitsuka, H. Kohguchi, M. Ehara and T. Ebata, *J. Phys. Chem. Lett.*, 2016, **7**, 4001–4007.
200 D. H. William and I. Fleming, *Spectroscopic Methods in Organic Chemistry*, McGraw-Hill Education, *London*, 6th edn, 2008.
201 K. M. Hanson, S. Narayanan, V. M. Nichols and C. J. Bardeen, *Photochem. Photobiol. Sci.*, 2015, **14**, 1607–1616.
202 T. M. Karpkird, S. Wanichweacharungruang and B. Albinsson, *Photochem. Photobiol. Sci.*, 2009, **8**, 1455–1460.
203 C.-X. Li, W.-W. Guo, B.-B. Xie and G. Cui, *J. Chem. Phys.*, 2016, **145**, 074308.
204 L. A. Baker, M. D. Horbury, S. E. Greenough, M. N. R. Ashfold and V. G. Stavros, *Photochem. Photobiol. Sci.*, 2015, **14**, 1814–1820.
205 M. T. Ignasiak, C. Houée-Levin, G. Kciuk, B. Marciniak and T. Pedzinski, *ChemPhysChem*, 2015, **16**, 628–633.
206 A. Cantrell and D. J. McGarvey, *J. Photochem. Photobiol., B*, 2001, **64**, 117–122.
207 A. D. Dunkelberger, R. D. Kieda, B. M. Marsh and F. F. Crim, *J. Phys. Chem. A*, 2015, **119**, 6155–6161.
208 M. Yamaji and M. Kida, *J. Phys. Chem. A*, 2013, **117**, 1946–1951.
209 M. D. Horbury, L. A. Baker, W.-D. Quan, J. D. Young, M. Staniforth, S. E. Greenough and V. G. Stavros, *J. Phys. Chem. A*, 2015, **119**, 11989–11996.

210 T. N. V. Karsili, A. M. Wenge, S. J. Harris, D. Murdock, J. N. Harvey, R. N. Dixon and M. N. R. Ashfold, *Chem. Sci.*, 2013, **4**, 2434–2446.
211 M. Gauden, A. Pezzella, L. Panzella, M. T. Neves-Petersen, E. Skovsen, S. B. Petersen, K. M. Mullen, A. Napolitano, M. d'Ischia and V. Sundström, *J. Am. Chem. Soc.*, 2008, **130**, 17038–17043.
212 N. K. Schwalb and F. Temps, *J. Am. Chem. Soc.*, 2007, **129**, 9272–9273.
213 L. R. Gaspar and P. M. B. G. Maia-Campos, *Int. J. Pharm.*, 2006, **307**, 123–128.
214 B. Herzog, M. Wehrle and K. Quass, *Photochemistry*, 2009, **85**, 869–878.
215 S. Afonso, K. Horita, J. P. Sousa e Silva, I. F. Almeida, M. H. Amaral, P. A. Lobão, P. C. Costa, M. S. Miranda, J. C. G. Esteves da Silva and J. M. Sousa Lobo, *J. Photochem. Photobiol., B*, 2014, **140**, 36–40.
216 V. Lhiaubet-Vallet, M. Marin, O. Jimenez, O. Gorchs, C. Trullas and M. A. Miranda, *Photochem. Photobiol. Sci.*, 2010, **9**, 552–558.
217 L. A. Baker, L. C. Grosvenor, M. N. R. Ashfold and V. G. Stavros, *Chem. Phys. Lett.*, 2016, **664**, 39–43.
218 J. Kockler, L. Oelgemöller, S. Robertson and B. D. Glass, *J. Photochem. Photobiol., C*, 2012, **13**, 91–110.
219 K. M. Hanson, E. Gratton and C. J. Bardeen, *Free Radical Biol. Med.*, 2006, **41**, 1205–1212.